Journal of Elasticity (2022) 151:273–303
https://doi.org/10.1007/s10659-022-09937-w

A Continuum Model for Circular Graphene Membranes Under Uniform Lateral Pressure

Matteo Pelliciari[1] · **Angelo Marcello Tarantino**[1]

Received: 7 March 2022 / Accepted: 21 September 2022 / Published online: 14 October 2022

Abstract
Despite the numerous applications of pressurized graphene membranes in new technologies, there is still a lack of accurate mechanical models. In this work we develop a continuum model for circular graphene membranes subjected to uniform lateral pressure. We adopt a semi-inverse method by defining a simplified kinematics of deformation and we describe the material behavior with a stored energy function that takes into account both nonlinearity and anisotropy of graphene. An expression of the applied pressure as a function of the deflection of the membrane is obtained from an approximate solution of the equilibrium. The simplifying hypotheses of the analytical model are verified by a finite element (FE) analysis in nonlinear elasticity. In addition, a numerical solution of the differential equilibrium equations of the exact theory is presented. The pressure-deflection response from FE and numerical solutions agree well with the prediction of the analytical formula, demonstrating its accuracy. The analytical solution is then employed for the response of a two-layered composite membrane made of graphene deposited onto a soft substrate. This application is of great interest since new nanotechnologies make use of layered nanocomposites. Differently from our entirely nonlinear approach, most continuum models in the literature are based on the assumption of linear elastic material, which is suitable only when deformations are small. The present work gives a comprehensive description of the mechanics of pressurized graphene membranes.

Keywords Graphene membranes · Nonlinear elasticity · Finite element · Nanocomposites

Mathematics Subject Classification (2010) 74B20 · 74G05 · 74K15 · 74S05 · 74E10

1 Introduction

Numerous applications in new technologies involve the use of graphene. The extraordinary mechanical, thermal and electrical properties of this material attracted the interest of

✉ M. Pelliciari
matteo.pelliciari@unimore.it

A.M. Tarantino
angelomarcello.tarantino@unimore.it

[1] DIEF, Department of Engineering “Enzo Ferrari”, via Pietro Vivarelli 10, 41125 Modena, Italy

researchers from many engineering fields. In fact, graphene is used in micro-and nano-electronic devices [56, 70], biomedicine [57], nanocomposite materials [16, 43, 55], energy generation and storage [51, 54], electrochemical sensors [27], and many other applications.

Graphene membranes are impermeable to standard gases and therefore they are often used for pressure sensors [5]. Pressurized graphene membranes provide a one-atom-thick separation barrier that can support large pressure differences. Liu et al. [36] reported the outstanding molecular separation properties of graphene membranes, which can be applied to pressure filtration, pervaporation and gas separation. Graphene membranes are also used as piezoresistive pressure sensors [72] and as pressure sensors for detecting human motions [59]. Wang et al. [63] presented a graphene-based microelectromechanical system (MEMS) pressure sensor and showed that, thanks to its high sensitivity, it outperforms most existing MEMS sensors. Moreover, polymer nanocomposite membranes based on graphene find new and promising technological applications [28, 41].

Despite the enormous potential of pressurized graphene membranes, there is still a lack of accurate mechanical models. Wang et al. [62] analyzed the problem of circular graphene membranes subjected to uniform lateral pressure and proposed approximate analytical solutions based on the assumption of linear elastic material. They carried out molecular dynamics simulations on a nanoscale membrane and it was found that the approximate solutions are suitable only for small deflections (linear elasticity). Jiang et al. [25] and Wang et al. [60] carried out FE simulations by modeling the graphene sheet with, respectively, plate and shell elements composed of linear elastic material. Li et al. [33] proposed a continuum model based on the large deflection elastic theory of circular membranes and investigated the effect of variations of the membrane parameters by using FE simulations.

The above models are all based on the hypothesis of linear elastic constitutive response of graphene. However, experiments and numerical simulations showed that graphene exhibits a pronounced material nonlinearity, which derives from the nonlinear carbon-carbon interactions in the hexagonal lattice [32, 37, 48, 50]. In addition, graphene is isotropic only for infinitesimal deformations, while in the theory of large deformations its anisotropy must be taken into account [24]. This behavior of graphene is not considered in the models mentioned above. Against this background, there are still important issues that must be addressed to provide a comprehensive description of the mechanics of circular pressurized graphene membranes.

In the present work, we address this problem in the framework of finite elasticity. We adopt a semi-inverse method by defining a simplified kinematics of deformation of the circular pressurized membrane. Consequently, we consider the anisotropic hyperelastic material model for graphene proposed by Höller et al. [23] and we derive the stress measures. The equilibrium is then written and an approximate solution is derived. Thereby, an expression of the applied pressure as a function of the deflection of the central point of the membrane is proposed. The simplifying hypotheses of the proposed analytical solution are verified by a FE simulation in nonlinear elasticity. The FE simulation was carried out in software COMSOL Multiphysics. Both material and geometric nonlinearities were considered.

As mentioned above, in order to derive an analytical solution, the equilibrium problem is written under a simplifying assumption on the kinematics of deformation. With the aim of providing a comprehensive investigation of the mechanics of pressurized graphene membranes, such assumption is abandoned and the differential equilibrium equations of the exact theory are derived. A numerical procedure to solve such system of equations is presented. The results from FE, numerical and analytical solutions are compared to show that the proposed pressure-deflection relation is accurate. We also present a comparison with other results from experiments and simulations found in the literature.

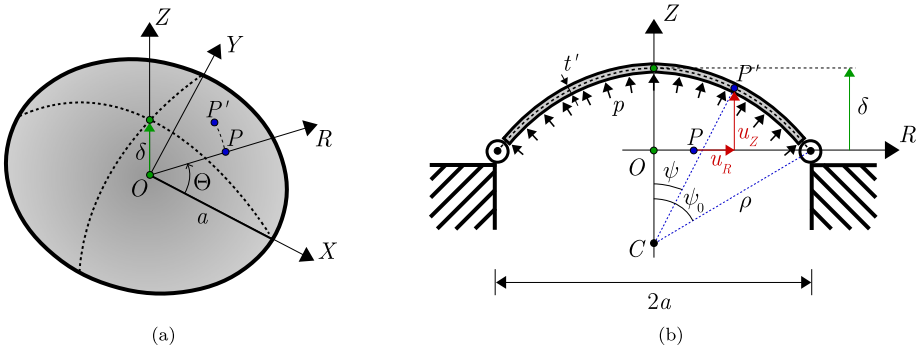

Fig. 1 (**a**) Circular graphene membrane subjected to uniform lateral pressure and (**b**) kinematics of deformation in the R-Z plane based on the assumption that the membrane transforms into a spherical cap with origin in C

The analytical solution is then employed for the prediction of the response of composite membranes made of graphene deposited on a soft substrate. This topic has gained more and more attention because of the numerous applications in new nanotechnologies (see, e.g, [10, 11, 13, 34, 58]). A pressure-deflection relation for a two-layered nanocomposite is proposed and the effect of graphene on the final response is investigated. An expression of the equivalent Young's modulus is derived from the linearized theory.

The paper is organized as follows. The hyperelastic model and the approximate analytical solution for circular graphene membranes under uniform lateral pressure are presented in Sect. 2. The FE model is described in Sect. 3 and the numerical solution of the equilibrium problem is presented in Sect. 4. The results are given in Sect. 5. The proposed analytical solution is firstly compared with the FE and numerical simulations and then with other results from the literature. In Sect. 6 we analyze the case of layered membranes composed of graphene deposited onto a soft surface. Conclusions are drawn in Sect. 7.

2 Hyperelastic Model and Approximate Analytical Solution

The circular pressurized graphene membrane is depicted in Fig. 1a. The undeformed flat membrane has radius a and thickness t. We introduce a Cartesian coordinate system (X, Y, Z) and a cylindrical coordinate system (R, Θ, Z), both with origin in O. Directions X and Y correspond respectively to zigzag and armchair directions in the graphene hexagonal lattice [6, 30]. The membrane is subjected to the uniform pressure p and material point P moves to P'. We assume that the membrane preserves its rotational symmetry after deformation, therefore $\Theta' = \Theta$. The coordinates of P' in deformed configuration are (R', Θ, Z').

We assume that the initially flat membrane transforms into a spherical cap. Note that the ultimate strain of graphene subjected to uniaxial elongation is around 15-20% [61, 67, 71]. Since the deformations involved are moderately large, the assumption that the membrane transforms into a spherical cap gives an appropriate description of the kinematics of deformation [69]. This hypothesis will be verified by the FE simulation in Sect. 3. We remark that in the present analysis the out-of-plane bending stiffness of graphene is ignored. The formulation is thus valid for deformation states in which the contribution of bending to the strain energy density is negligible compared to that of the in-plane deformation. In light of this,

the linear behavior at small deflections is not well captured because, in such circumstance, graphene behaves as an elastic plate instead of a membrane.

The membrane deforms according to the kinematics of Fig. 1b. The spherical cap is centered in point C and has radius ρ. Displacement field $\mathbf{u}(P)$ of point P with coordinates $(R, \Theta, 0)$ has the following expression in cylindrical coordinates:

$$\begin{aligned} u_R(P) &= R' - R = \rho \sin\psi - R, \\ u_\Theta(P) &= 0, \\ u_Z(P) &= Z' = \rho\,(\cos\psi - \cos\psi_0)\,, \end{aligned}$$

where $\psi_0 \in (0, \pi)$ and

$$\rho = \frac{a}{\sin\psi_0}, \qquad \psi = \frac{\psi_0 R}{a}.$$

The deformation of point P is $\boldsymbol{\varphi}(P) = \mathbf{id}(P) + \mathbf{u}(P)$[1] and its representation in cylindrical coordinates is

$$\begin{aligned} \varphi_R(P) &= \rho \sin\psi, \\ \varphi_\Theta(P) &= \Theta, \\ \varphi_Z(P) &= \rho\,(\cos\psi - \cos\psi_0)\,. \end{aligned}$$

In order to derive the deformation gradient $\mathbf{F}$ we must introduce the contraction of the membrane thickness, which is expressed by stretch λ_Z. However, we are considering a single-layer graphene sheet whose thickness corresponds to the diameter of the carbon atom. From a physical point of view it is hard to imagine that such thin membrane can undergo a transverse contraction, because this would produce a reduction of the dimension of the atom. In light of this, the most reasonable assumption is that $\lambda_Z = 1$ throughout the deformation process, which means that thickness t of the undeformed membrane remains unchanged ($t' = t$). In this section we proceed according to such an assumption. However, the lack of experimental observation does not allow to validate this hypothesis. Hence, we also propose a solution considering the transverse contraction, which is outlined in Appendix A. The results from both solutions will be presented and compared. It is remarked that the most common hypothesis for graphene is that $\lambda_Z = 1$ [40]. Nevertheless, the solution in Appendix A may be a good basis for continuum models of multilayer graphene, where transverse contraction certainly plays a role.

Under the assumption that $\lambda_Z = 1$, the deformation gradient is derived as follows [46]:

$$[\mathbf{F}] = \begin{bmatrix} \dfrac{\partial\varphi_R}{\partial R} & \dfrac{1}{R}\dfrac{\partial\varphi_R}{\partial\Theta} & \sin\psi \\ \varphi_R\dfrac{\partial\varphi_\Theta}{\partial R} & \dfrac{\varphi_R}{R}\dfrac{\partial\varphi_\Theta}{\partial\Theta} & 0 \\ \dfrac{\partial\varphi_Z}{\partial R} & \dfrac{1}{R}\dfrac{\partial\varphi_Z}{\partial\Theta} & \cos\psi \end{bmatrix} = \begin{bmatrix} \rho\dfrac{\partial\psi}{\partial R}\cos\psi & 0 & \sin\psi \\ 0 & \dfrac{\rho\sin\psi}{R} & 0 \\ -\rho\dfrac{\partial\psi}{\partial R}\sin\psi & 0 & \cos\psi \end{bmatrix}.$$

[1] $\mathbf{id}(P)$ indicates the position vector of point P.

The polar decomposition of the deformation gradient, $\mathbf{F} = \mathbf{R}\mathbf{U}$, allows us to write rotation tensor $\mathbf{R}$ and right stretch tensor $\mathbf{U}$ as

$$[\mathbf{R}] = \begin{bmatrix} \cos\psi & 0 & \sin\psi \\ 0 & 1 & 0 \\ -\sin\psi & 0 & \cos\psi \end{bmatrix}, \qquad [\mathbf{U}] = \begin{bmatrix} \rho\dfrac{\partial\psi}{\partial R} & 0 & 0 \\ 0 & \dfrac{\rho\sin\psi}{R} & 0 \\ 0 & 0 & 1 \end{bmatrix}. \tag{1}$$

Tensor $\mathbf{U}$ is diagonal and therefore the cylindrical coordinate system (R, Θ, Z) is principal. Hence, from (1) we derive the following expressions of the principal stretches:

$$\lambda_R = \rho\frac{\partial\psi}{\partial R} = \frac{\rho\psi_0}{a}, \qquad \lambda_\Theta = \frac{\rho\sin\psi}{R}. \tag{2}$$

Radial stretch λ_R is not a function of position because we assumed that the membrane deforms into a spherical cap.

The right Cauchy-Green deformation tensor, $\mathbf{C} = \mathbf{F}^T\mathbf{F}$, is computed and expressed in cylindrical coordinates as

$$[\mathbf{C}] = \begin{bmatrix} \lambda_R^2 & 0 & 0 \\ 0 & \lambda_\Theta^2 & 0 \\ 0 & 0 & 1 \end{bmatrix},$$

with λ_R and λ_Θ given by (2). The Green-Lagrange strain tensor, $\mathbf{E} = (\mathbf{C} - \mathbf{I})/2$, has the following diagonal form:

$$[\mathbf{E}] = \begin{bmatrix} E_R & 0 & 0 \\ 0 & E_\Theta & 0 \\ 0 & 0 & E_Z \end{bmatrix} = \frac{1}{2}\begin{bmatrix} \lambda_R^2 - 1 & 0 & 0 \\ 0 & \lambda_\Theta^2 - 1 & 0 \\ 0 & 0 & 0 \end{bmatrix}. \tag{3}$$

The extensive number of investigations on the mechanical behavior of graphene demonstrated that this material is isotropic only for small deformations, while anisotropy arises when deformations become large [24, 42]. This is due to the particular symmetry and periodicity of the graphene honeycomb lattice. To this regard, Kumar and Parks [31] used the isotropicization theorem [53] to define an additional invariant of the Green-Lagrange strain tensor that reproduces the anisotropic nature of graphene. We introduce tensors $\mathbf{M} = \mathbf{n}_X \otimes \mathbf{n}_X - \mathbf{n}_Y \otimes \mathbf{n}_Y$[2] and $\mathbf{N} = \mathbf{n}_X \otimes \mathbf{n}_Y + \mathbf{n}_Y \otimes \mathbf{n}_X$, which define the material symmetry group of graphene. Thereby, the strain energy density of graphene is written as a function of the following strain invariants:

$$\begin{aligned} I_1 &= \mathrm{tr}\mathbf{E} = E_R + E_\Theta, \\ I_2 &= \frac{1}{2}\left[(\mathrm{tr}\mathbf{E})^2 - \mathrm{tr}\left(\mathbf{E}^2\right)\right] = E_R E_\Theta, \\ I_3 &= (\mathbf{M}\cdot\mathbf{E})^3 - 3\,(\mathbf{M}\cdot\mathbf{E})\,(\mathbf{N}\cdot\mathbf{E})^2 = (E_R - E_\Theta)^3\cos(6\phi)\,, \end{aligned} \tag{4}$$

where $\phi \in [0, \pi/6]$ and it represents the angle that principal direction 1 forms with zigzag direction (Fig. 2). Symmetry and periodicity of graphene allows us to investigate its material

[2]Unit vectors $\mathbf{n}_X$ and $\mathbf{n}_Y$ identify respectively directions X and Y of the Cartesian coordinate system. Symbols $\otimes$ and $(\cdot)$ denote dyadic product and second-order tensor contraction, respectively.

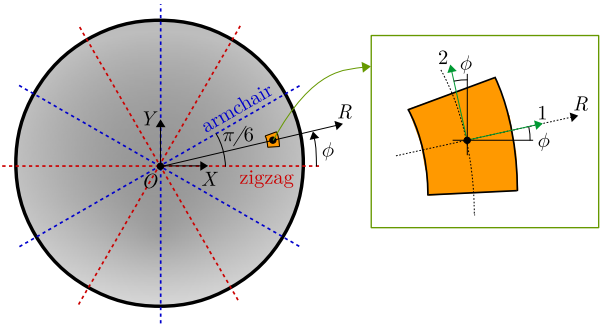

Fig. 2 Representation of the periodicity in the lattice structure of graphene, which repeats itself allowing to study its mechanical response within the domain identified by $\phi \in [0, \pi/6]$

behavior in the domain between zigzag and armchair directions, inside which $\phi = \Theta$. Note that, in (4), I_1 and I_2 are the isotropic principal invariants of the Green-Lagrange strain tensor [47]. Anisotropy is introduced with the third invariant I_3, which plays a role only when deformations are relatively large and $E_R \neq E_\Theta$. Equation (4) is rewritten as a function of the principal stretches as follows:

$$\begin{aligned} I_1 &= \frac{1}{2}\left(\lambda_R^2 + \lambda_\Theta^2 - 2\right), \\ I_2 &= \frac{1}{4}\left(\lambda_R^2 - 1\right)\left(\lambda_\Theta^2 - 1\right), \\ I_3 &= \frac{1}{8}\left(\lambda_R^2 - \lambda_\Theta^2\right)^3 \cos\left(6\phi\right). \end{aligned} \tag{5}$$

In general, circular membranes composed of anisotropic materials lose their rotational symmetry when subjected to uniform lateral pressure. Nevertheless, this effect is negligible for the particular case of graphene and the reason is as follows. As already pointed out, graphene breaks for deformations that are not very large. The ultimate value of strain is reached before that invariant I_3 assumes a sensible importance. Specifically, term $\left(\lambda_R^2 - \lambda_\Theta^2\right)^3$ is negligible with respect to the values assumed by the isotropic invariants I_1 and I_2. Given the above, the hypothesis of axisymmetric kinematics of deformation is still valid and gives a simplified but effective description of the actual behavior of graphene. In any case, this assumption will be verified by the FE simulation, which will be presented in Sect. 3. This hypothesis on the kinematics makes it possible to derive a pressure-deflection relation for the membrane problem. This clarifies the necessity and effectiveness of such assumption.

In this work, we consider the stored energy function for graphene introduced by Höller et al. [23] by fitting density functional theory (DFT) simulations. Subsequent works [45, 49] showed its validity and accuracy in the prediction of the graphene response subjected to large in-plane deformations. In particular, in [45], a new set of constitutive parameters was calibrated by fitting FE molecular mechanics simulations under both uniaxial and equibiaxial loads. The hyperelastic model provided accurate predictions of the graphene mechanics and therefore we consider the constitutive parameters proposed in such work. It goes without saying that there are other hyperelastic models for graphene in the literature (see, e.g., [31, 64, 65]). Also these models have been proven to provide accurate and reliable predictions of the graphene mechanics. The choice of the constitutive function in this work was mainly driven by its particularly straightforward mathematical description.

The stored energy function proposed in [23] is

$$\omega(I_1, I_2, I_3) = \frac{1}{t}\sum_{k=1}^{3} c_k I_k + \frac{1}{t}\sum_{h=1}^{11} c_{h+3} J_h, \tag{6}$$

where $c_1 - c_{14}$ are polynomial fitting coefficients with dimension of energy per unit area, whose values are reported in Table 3 of work [45]. Invariants J_h are defined as polynomial combinations of I_1, I_2 and I_3 and their expressions are given in [23]. Being graphene a one-atom-thick layer, it is often treated as a two-dimensional material. In the expression of the stored energy function (6), we divided by thickness t so as to regard the graphene membrane as a three-dimensional solid and evaluate stress components with the usual dimension of force per unit area.

The second Piola-Kirchhoff stress tensor is energetically conjugated to the Green-Lagrange strain tensor and thus it is computed as

$$\mathbf{\Sigma} = \frac{\partial \omega}{\partial \mathbf{E}}(I_1, I_2, I_3) = \sum_{k=1}^{3} \frac{\partial \omega}{\partial I_k}\frac{\partial I_k}{\partial \mathbf{E}}, \tag{7}$$

where the derivatives of the principal invariants with respect to $\mathbf{E}$ are

$$\frac{\partial I_1}{\partial \mathbf{E}} = \mathbf{n}_X \otimes \mathbf{n}_X + \mathbf{n}_Y \otimes \mathbf{n}_Y, \quad \frac{\partial I_2}{\partial \mathbf{E}} = I_1\left(\mathbf{n}_X \otimes \mathbf{n}_X + \mathbf{n}_Y \otimes \mathbf{n}_Y\right) - \mathbf{E}, \quad \frac{\partial I_3}{\partial \mathbf{E}} = \mathbf{S},$$

with $\mathbf{S} = 3\left[(\mathbf{M}\cdot\mathbf{E})^2 - (\mathbf{N}\cdot\mathbf{E})^2\right]\mathbf{M} - 6\left[(\mathbf{M}\cdot\mathbf{E})(\mathbf{N}\cdot\mathbf{E})\right]\mathbf{N}$, whose representation in the cylindrical coordinate system is

$$[\mathbf{S}] = 3\left(E_R - E_\Theta\right)^2 \begin{bmatrix} \cos(6\phi) & -\sin(6\phi) & 0 \\ -\sin(6\phi) & -\cos(6\phi) & 0 \\ 0 & 0 & 0 \end{bmatrix}.$$

We introduce invariants β_1, β_2 and β_3, defined as

$$\begin{aligned}
\beta_1 &= c_1 + c_2 I_1 - 3c_5 I_2 + c_6\left(I_1^2 + I_2\right) - 4c_7 I_1 I_2 + 2c_8 I_1 I_2 + c_9\left(I_1^3 - 2I_1 I_2\right) \\
&\quad + 5c_{10}\left(I_2^2 - I_1^2 I_2\right) + c_{11}\left(I_1^4 - 3I_2^2 - 3I_1^2 I_2\right) + c_{12}\left(I_2^2 + 2I_1^2 I_2\right) + c_{13} I_3, \\
\beta_2 &= -c_2 + 2c_4 + 3c_5 I_1 - c_6 I_1 + 4c_7\left(I_1^2 - I_2\right) - 2c_8 I_2 + c_9\left(4I_2 - I_1^2\right) \\
&\quad + 5c_{10}\left(I_1^3 - 2I_1 I_2\right) + c_{11}\left(6I_1 I_2 - I_1^3\right) - 2c_{12} I_1 I_2 + 2c_{14} I_3, \\
\beta_3 &= c_3 + c_{13} I_1 + c_{14}\left(I_1^2 - 2I_2\right).
\end{aligned} \tag{8}$$

From (7) we derive the following expressions for the components of the symmetric second Piola-Kirchhoff stress tensor:

$$\begin{aligned}
\Sigma_{RR} &= \frac{\beta_1}{t} + \frac{\beta_2}{2t}\left(\lambda_R^2 - 1\right) + \frac{3\beta_3}{4t}\left(\lambda_R^2 - \lambda_\Theta^2\right)^2 \cos(6\phi), \\
\Sigma_{\Theta\Theta} &= \frac{\beta_1}{t} + \frac{\beta_2}{2t}\left(\lambda_\Theta^2 - 1\right) - \frac{3\beta_3}{4t}\left(\lambda_R^2 - \lambda_\Theta^2\right)^2 \cos(6\phi), \\
\Sigma_{R\Theta} &= -\frac{3\beta_3}{4t}\left(\lambda_R^2 - \lambda_\Theta^2\right)^2 \sin(6\phi), \\
\Sigma_{RZ} &= \Sigma_{\Theta Z} = \Sigma_{ZZ} = 0.
\end{aligned} \tag{9}$$

It is assumed that the graphene undeformed configuration is stress free and therefore $c_1 = 0$.

Having at hand the second Piola-Kirchhoff stress tensor, the other stress measures can be derived. The first Piola-Kirchhoff stress tensor, $\mathbf{T}_R = \mathbf{F}\boldsymbol{\Sigma}$, reads

$$[\mathbf{T}_R] = \begin{bmatrix} \lambda_R \Sigma_{RR} \cos\psi & \lambda_R \Sigma_{R\Theta} \cos\psi & 0 \\ \lambda_\Theta \Sigma_{R\Theta} & \lambda_\Theta \Sigma_{\Theta\Theta} & 0 \\ -\lambda_R \Sigma_{RR} \sin\psi & -\lambda_R \Sigma_{R\Theta} \sin\psi & 0 \end{bmatrix}. \tag{10}$$

We observe that $\mathbf{T}_R \mathbf{n}_Z = \mathbf{0}$. This guarantees that the stress component normal to the deformed membrane is zero, as required by the membrane stress state. $\mathbf{T}_R$ is not diagonal in reference system (R, Θ, Z), which is principal regarding the deformation. Hence, the principal strain directions do not coincide with the principal stress directions. This is not a surprise given that graphene is described by an anisotropic material model. In order to write the equilibrium in deformed configuration, we now derive the Cauchy stress tensor $\mathbf{T} = \mathbf{T}_R \mathbf{F}^T / \det\mathbf{F}$. By definition, tensor $\mathbf{T}$ is symmetric and its components are

$$\begin{aligned} &T_{RR} = \frac{\lambda_R}{\lambda_\Theta} \Sigma_{RR} \cos^2\psi, \qquad T_{\Theta\Theta} = \frac{\lambda_\Theta}{\lambda_R} \Sigma_{\Theta\Theta}, \qquad T_{ZZ} = \frac{\lambda_R}{\lambda_\Theta} \Sigma_{RR} \sin^2\psi, \\ &T_{R\Theta} = \Sigma_{R\Theta} \cos\psi, \qquad T_{RZ} = -\frac{\lambda_R}{\lambda_\Theta} \Sigma_{RR} \cos\psi \sin\psi, \qquad T_{\Theta Z} = -\Sigma_{R\Theta} \sin\psi. \end{aligned} \tag{11}$$

At this point, the equilibrium allows us to derive a relationship between applied pressure and deflection of the membrane. We adopted a semi-inverse approach, with which we set an appropriate kinematics of deformation and accordingly we obtained the stress tensors. The kinematics of the model is not exact and thus the local equilibrium equations can not be solved in every internal point of the membrane. The exact solution to the local equilibrium is not known and it would include a more general kinematics. Nevertheless, we derive an approximate analytical solution by imposing the equilibrium between applied pressure and internal stresses in the neighborhood of the central point of the membrane. With this aim, we firstly compute the Cauchy stress tensor for the limit case of $R \to 0$. In this circumstance, radial and circumferential stretches are equal to each other ($\lambda_R = \lambda_\Theta|_{R\to 0} = \lambda$). Third invariant I_3 goes to zero and the only non-zero components of the Cauchy stress tensor are

$$T_{RR}|_{R\to 0} = T_{\Theta\Theta}|_{R\to 0} = T_0 = \frac{1}{t}\, \beta_1|_{R\to 0} + \frac{1}{2t} \left(\psi_0^2 \csc\psi_0^2 - 1\right) \beta_2|_{R\to 0}\,. \tag{12}$$

In the neighborhood of the central point, equilibrium along Z direction reads

$$p\left(\pi\rho^2 d\psi^2\right) = T_0 \left(2\pi\rho d\psi t\right) d\psi,$$

from which we derive the following relationship between lateral pressure and kinematic parameter ρ:

$$p = \frac{2T_0 t}{\rho}. \tag{13}$$

Using (12), (8) and (5) and recalling that $\rho = a/\sin\psi_0$, equation (13) takes the form

$$p = \frac{1}{8a} \sin\psi_0 \sum_{j=1}^{4} \kappa_j \left(\psi_0^2 \csc^2\psi_0 - 1\right)^j, \tag{14}$$

where

$$\kappa_1 = 8\,(c_2 + 2c_4)\,, \quad \kappa_2 = 12\,(c_5 + c_6)\,, \quad \kappa_3 = 4\,(2c_7 + c_8 + 2c_9)\,,$$
$$\kappa_4 = 5\,(c_{10} + c_{11} + c_{12})\,.$$

Angle ψ_0 is related to displacement δ of the central node through $\psi_0 = 2\arctan\bar{\delta}$, with $\bar{\delta} = \delta/a$ denoting the normalized deflection. By substitution into (14), the pressure-deflection relation for circular graphene membranes is finally obtained.

2.1 Linearized Formulation

Graphene is isotropic when deformations are small. Hence, in linear elasticity its material behavior is entirely described by two constants: Young's modulus E and Poisson's ratio ν. Expressions for E and ν can be derived from the finite theory by introducing the hypothesis that both displacements and displacement gradients are small [9, 18]. To this aim, strain and stress measures are developed in Taylor series as functions of ψ_0 and they are truncated at the second order. The Green-Lagrange strain tensor, expressed by (3), assumes the following linearized expression:

$$[\mathbf{E}] \cong \begin{bmatrix} \dfrac{\psi_0^2}{6} & 0 & 0 \\ 0 & \dfrac{(a-R)(a+R)\psi_0^2}{6a^2} & 0 \\ 0 & 0 & 0 \end{bmatrix}. \tag{15}$$

Tensor $\mathbf{E}$ is the infinitesimal strain tensor in the classical linear theory.

The linearization of the second Piola-Kirchhoff stress tensor $\mathbf{\Sigma}$, given by (9), provides

$$[\mathbf{\Sigma}] \cong \begin{bmatrix} \dfrac{\psi_0^2}{6t}\left[\left(1 - \dfrac{R^2}{a^2}\right)c_2 + 2c_4\right] & 0 & 0 \\ 0 & \dfrac{\psi_0^2}{6t}\left[c_2 + 2\left(1 - \dfrac{R^2}{a^2}\right)c_4\right] & 0 \\ 0 & 0 & 0 \end{bmatrix}. \tag{16}$$

The development in Taylor series of both $\mathbf{T_R}$ and $\mathbf{T}$ (equations (11) and (10) respectively), with truncation at the second order in ψ_0, gives the same result as (16). Therefore, as it should be, in the linearized theory all the stress measures coincide and we may refer only to a single stress tensor, expressed by (16). Furthermore, we notice that the representation of the stress tensor in the principal strain system is diagonal. This indicates that in the linearized theory principal strain and stress directions coincide. This because graphene is isotropic for small deformations.

The Navier's constitutive relationships for plane stress are

$$\begin{aligned} \sigma_R &= \frac{E}{1-\nu^2}\,(\epsilon_R + \nu\epsilon_\Theta)\,, \\ \sigma_\Theta &= \frac{E}{1-\nu^2}\,(\epsilon_\Theta + \nu\epsilon_R)\,. \end{aligned} \tag{17}$$

Stress components σ_R and σ_Θ are given respectively by the radial and circumferential components of the linearized stress tensor (16). Same goes for strain components ϵ_R and ϵ_Θ,

which are expressed by the strain tensor (15). Equation (17) transforms into the following linear system of two equations in the two unknown variables E and ν:

$$\frac{8a^2c_4 + 4c_2(a-R)(a+R)}{t} + \frac{E\left[4a^2(\nu+1) - 4\nu R^2\right]}{\nu^2 - 1} = 0,$$
$$\frac{4a^2c_2 + 8c_4(a-R)(a+R)}{t} + \frac{E\left[4a^2(\nu+1) - 4R^2\right]}{\nu^2 - 1} = 0,$$

whose solution gives the expressions of the elastic constants of graphene in linear elasticity

$$E = \frac{1}{t}\left(2c_4 - \frac{c_2^2}{2c_4}\right), \quad \nu = \frac{c_2}{2c_4}. \tag{18}$$

This result corresponds to that derived by Höller et al. [23]. Under the hypothesis of homogeneous deformations, the authors obtained the expression of the tangent elasticity tensor. The linearization of such tensor with $\mathbf{E} \to \mathbf{0}$ provided the Young's modulus and Poisson's ratio given in (18).

The linearized form of the pressure-deflection relation is obtained by developing (14) in Taylor series as function of ψ_0 and truncating at the third order. Constitutive parameters c_2 and c_4 are written as functions of E and ν by using (18). The following expression is derived:

$$p = \frac{8Et}{3a\,(1-\nu)} \arctan^3 \bar{\delta}. \tag{19}$$

3 Finite Element Simulation

The formulation presented in the previous section is based on the following assumptions on the kinematics of deformation: (i) The deformed membrane preserves rotational symmetry; (ii) The membrane transforms into a spherical cap. Such assumptions allowed us to derive an approximate expression for the pressure-deflection relation. In this section, we present a FE analysis with the aim of verifying the validity of the above assumptions.

The FE model was realized by using software COMSOL Multiphysics version 6.0. The 3D membrane interface of the structural mechanics module was selected. This interface allows to model plane stress elements without bending stiffness that can deform both in the in-plane and out-of-plane directions.

The geometry of the membrane was defined through a work plane, in which a circle with radius $a = 2.375$ μm was built. This value of a is the one considered in the experimental and numerical investigations of works [25, 29, 60]. We will present comparisons of the results in the next section. The thickness of the membrane was set to $t = 0.335$ nm. A fixed constraint was assigned along the perimeter. This reproduces the condition for which, along the constrained geometry, displacements are zero in all directions. A pressure load was applied to the free face of the membrane. The pressure load is a follower load, therefore its direction changes with deformation in the geometrically nonlinear analysis.

In the COMSOL membrane analysis it is necessary to apply a tensile prestress. This in order to avoid the singularity due to the fact that the undeformed membrane has no transverse stiffness. In our model, the prestress was introduced as an external in-plane force of 0.001 N/m, which is negligible compared to the stress values acting in the graphene membrane

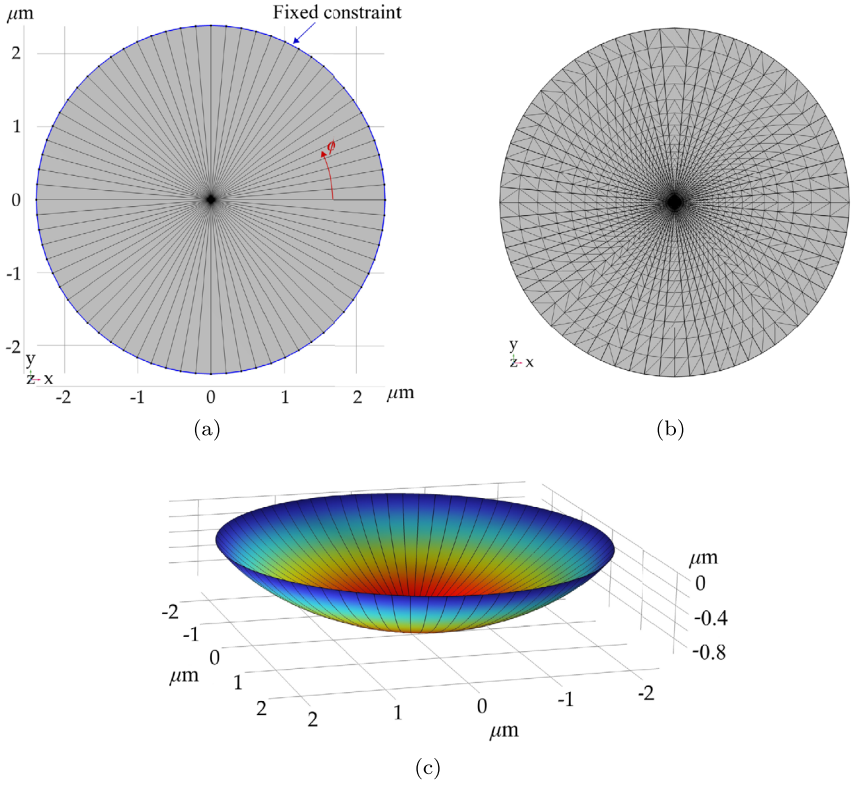

Fig. 3 FE simulation with COMSOL Multiphysics: (**a**) Subdivided domain to define the anisotropic material properties of graphene; (**b**) Mesh used for the analysis; (**c**) Deformed configuration of the circular graphene membrane after application of a uniform lateral pressure

during the simulation. The sole scope of the prestress was to avoid the singularity and allow the solver to find a solution.

The material behavior was defined through the user-defined compressible hyperelastic material. In detail, the isotropic invariants were introduced as local variables according to (4). Anisotropy was added by subdividing the domain into subdomains. To do this, the membrane was cut by planes parallel to direction Z and containing central point O. Starting from direction X, a plane was defined for every angle increment of 5 degrees (see Fig. 3a). The entire domain was thus partitioned into 72 subdomains. In each of them, invariant I_3 was defined as a local variable with the corresponding value of $\cos(6\phi)$. In other words, the variation of term $\cos(6\phi)$ in the expression of I_3 was introduced in a discrete way by subdividing the membrane domain into several subdomains. It goes without saying that this is a simplification, but it gives a reasonable approximation of the continuous variation of I_3 as a function of ϕ. One may further subdivide the domain in order to reach more accuracy, but as we will see in the following the contribution of graphene anisotropy is negligible in the problem analyzed. The subdivision into 72 subdomains is already enough.

The mesh was composed of triangular elements with minimum and maximum size of, respectively, 0.019 and 0.26 μm (Fig. 3b). A stationary simulation was carried out and the applied pressure was increased from 5 Pa to 18 MPa. The stationary solver MUMPS was

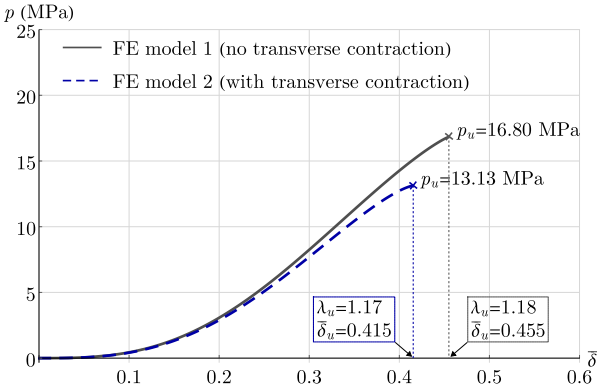

Fig. 4 Pressure-deflection curves, with $\bar{\delta} = \delta/a$, obtained from the FE analysis of a circular graphene sheet with radius 2.375 μm. The setup of FE model 1 is such as to avoid transverse contraction of graphene, while it is included in FE model 2. The ultimate pressure, normalized deflection and stretch at the pole are denoted by p_u, $\bar{\delta}_u$ and λ_u, respectively

employed. Figure 3c shows the deformed configuration of the circular graphene membrane for a certain value of applied pressure.

The 3D membrane model in COMSOL involves transverse contraction of the membrane. In order to avoid this, the term $c_\infty (\lambda_Z - 1)^2$ was added to the energy density function introduced in the user-defined compressible hyperelastic material. The value of parameter c_∞ was set as three orders of magnitude larger than the maximum value among parameters $c_1 - c_{14}$. In this way the membrane was much stiffer in Z direction and the values of the corresponding component of deformation were negligible with respect to both radial and circumferential deformations. This FE model setup is consistent with the hypothesis of the analytical solution presented in the previous section and, from now on, it will be referred as FE model 1. Another simulation was carried out after removing term $c_\infty (\lambda_Z - 1)^2$. This setup involves transverse contraction of the membrane and therefore it is consistent with the solution outlined in Appendix A. This second model will be referred as FE model 2.

The pressure-deflection curves obtained from the FE analysis are displayed in Fig. 4. The simulation of FE model 1 stopped at the ultimate value of pressure $p_u = 16.80$ MPa because an unstable (buckling) equilibrium configuration was reached. Namely, further increasing deflections require decreasing values of pressure to guarantee equilibrium. The ultimate value of stretch at the pole is $\lambda_u = 1.18$, which corresponds to the ultimate normalized displacement $\bar{\delta}_u = 0.455$. Same goes for FE model 2, but the ultimate value of pressure is $p_u = 13.13$ MPa, which took place at $\lambda_u = 1.17$ and $\bar{\delta}_u = 0.415$.

Although the stress state in the FE simulation is not equibiaxial, the value of λ_u is consistent with results in the literature obtained from simulations of graphene under equibiaxial loads. For instance, Cao et al. [7] and Marianetti and Yevick [39] carried out density functional theory (DFT) simulations and reported an ultimate strain close to 0.15. Yazdani and Hatami [68] and Pelliciari et al. [45] obtained from molecular mechanics simulations the ultimate strains 0.20 and 0.18, respectively. Note that the variability of the results in the literature is due to the different computational methods and interatomic potentials.

Figure 5 shows the profiles of deformation from FE model 1 along diameters identified by different angles ϕ. We observe that variations of ϕ do not cause appreciable variations in the deformed shape, represented in the R-Z plane. This means that the three-dimensional deformed configuration is axisymmetric with respect to Z. Figure 6a shows normalized displacement u_Z/a in the X-Y plane for the ultimate value of pressure computed by FE model 1. Figures 6b–6d show respectively the trend of invariants I_1, I_2 and I_3 in the membrane domain. The values of I_3 are very close to zero in the entire domain, except from the areas close to the perimeter. This because in such areas, due to the influence of the constrained

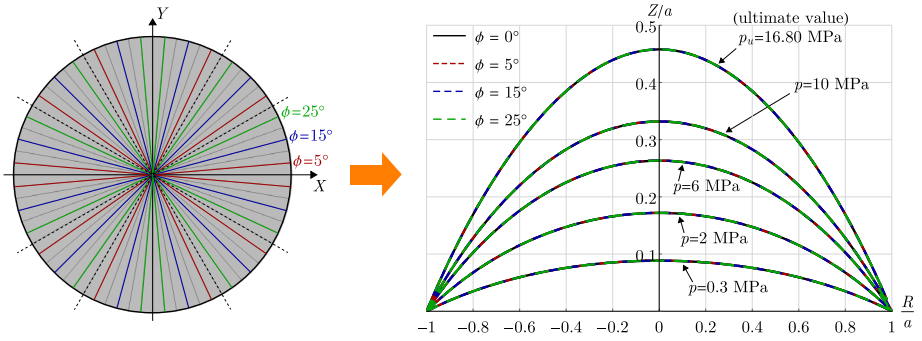

Fig. 5 Profiles of deformation from FE model 1 represented in the R-Z plane and given in terms of dimensionless coordinates R/a and Z/a ($a = 2.375$ μm). The deformed shapes along diameters with different angle ϕ coincide and therefore the kinematics of deformation is axisymmetric

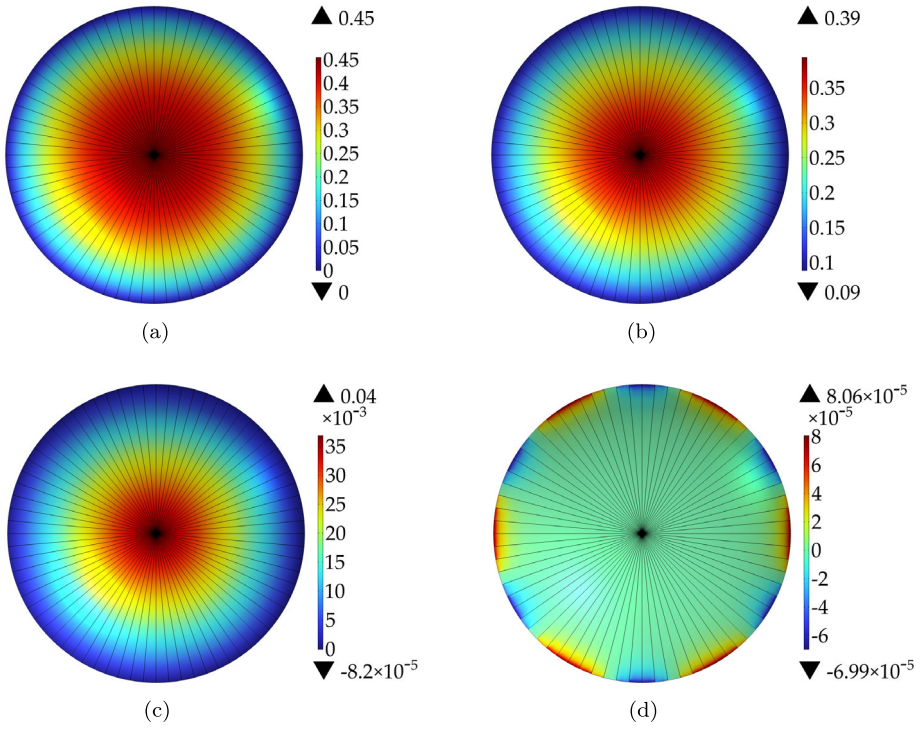

Fig. 6 Contour plots of (**a**) normalized deflection u_Z/a, (**b**) invariant I_1, (**c**) invariant I_2 and (**d**) invariant I_3 at the ultimate value of pressure from FE model 1. The values of I_3 are negligible with respect to both I_1 and I_2 and thus anisotropy of graphene does not activate

boundary, stretches λ_R and λ_Θ differ more than in the inner region. Nevertheless, the values assumed by I_3 are negligible with respect to I_1 and I_2 and therefore anisotropy of graphene does not play a noticeable role. The above discussion demonstrates that the assumption of

rotational symmetry in the analytical solution is accurate and in accordance with the FE simulation.

The profiles of deformation and the contour plots of deflection and invariants from FE model 2 show the same trend. Hence, even when considering transverse contraction, the deformed configurations preserve rotational symmetry. The corresponding results are not presented for the sake of brevity.

4 Numerical Solution of the Equilibrium Problem

In this section we present a numerical solution of the equilibrium problem of circular graphene membranes subjected to uniform lateral pressure. The pressure-deflection formula (14) was derived under the simplifying hypothesis that the membrane transforms into a spherical cap. Such hypothesis is now abandoned and the differential equilibrium equations are written. Then, a numerical procedure to solve such system of equations is presented.

The FE analysis allowed us to conclude that, for the problem analyzed in this paper, the role of graphene anisotropy is negligible. Hence, we keep the hypothesis that the deformed configuration preserves its rotational symmetry and, when computing the stress quantities, we neglect the terms related to I_3. As we did in Sect. 2, we assume that graphene does not undergo transverse contraction ($\lambda_Z = 1$). Thereby, the most general kinematics of deformation is described by the following deformation gradient [44]:

$$[\mathbf{F}] = \begin{bmatrix} \varphi'_R & 0 & -\dfrac{\varphi'_Z}{\sqrt{{\varphi'_R}^2 + {\varphi'_Z}^2}} \\ 0 & \dfrac{\varphi_R}{R} & 0 \\ \varphi'_Z & 0 & \dfrac{\varphi'_R}{\sqrt{{\varphi'_R}^2 + {\varphi'_Z}^2}} \end{bmatrix},$$

where $'$ denotes the derivative with respect to coordinate R. The dependence of the quantities with radial coordinate R is omitted for the sake of simplicity. The polar decomposition of the deformation gradient reads

$$[\mathbf{R}] = \frac{1}{\sqrt{{\varphi'_R}^2 + {\varphi'_Z}^2}} \begin{bmatrix} \varphi'_R & 0 & -\varphi'_Z \\ 0 & \sqrt{{\varphi'_R}^2 + {\varphi'_Z}^2} & 0 \\ \varphi'_Z & 0 & \varphi'_R \end{bmatrix},$$

$$[\mathbf{U}] = \begin{bmatrix} \sqrt{{\varphi'_R}^2 + {\varphi'_Z}^2} & 0 & 0 \\ 0 & \dfrac{\varphi_R}{R} & 0 \\ 0 & 0 & 1 \end{bmatrix}.$$

Hence, the principal stretches are expressed by

$$\begin{aligned} \lambda_R &= \sqrt{{\varphi'_R}^2 + {\varphi'_Z}^2}, \\ \lambda_\Theta &= \frac{\varphi_R}{R}. \end{aligned} \tag{20}$$

The equilibrium equations in radial and normal directions read [1]

$$\begin{aligned} \frac{dN_1}{d\varphi_R} + \frac{1}{\varphi_R}(N_1 - N_2) = 0, \\ K_1 N_1 + K_2 N_2 = p, \end{aligned} \tag{21}$$

where K_1 and K_2 are the principal curvatures in radial and circumferential directions respectively, while N_1 and N_2 are the principal stress resultants with dimension of force per unit length. The principal curvatures are written as [66]

$$K_1 = \frac{\lambda_R' w - \lambda_R w'}{\lambda_R^2 \sqrt{\lambda_R^2 - w^2}}, \quad K_2 = \frac{\sqrt{\lambda_R^2 - w^2}}{\lambda_R \lambda_\Theta R}, \tag{22}$$

where $w = \varphi_R'$. Neglecting anisotropy in (7), we express the components of the second Piola-Kirchhoff stress tensor as

$$\begin{aligned} &\Sigma_{RR} = \frac{\beta_1}{t} + \frac{\beta_2}{2t}\left(\lambda_R^2 - 1\right), \qquad \Sigma_{\Theta\Theta} = \frac{\beta_1}{t} + \frac{\beta_2}{2t}\left(\lambda_\Theta^2 - 1\right), \\ &\Sigma_{R\Theta} = \Sigma_{RZ} = \Sigma_{\Theta Z} = \Sigma_{ZZ} = 0. \end{aligned}$$

Since anisotropy is now neglected, principal directions of strain and stress coincide and thus tensor $\mathbf{\Sigma}$ is diagonal. The Cauchy stress tensor is computed as $\mathbf{T} = \mathbf{F}\mathbf{\Sigma}\mathbf{F}^T/\det\mathbf{F}$. The principal stress components in deformed configuration are derived by the transformation $\tilde{\mathbf{T}} = \mathbf{R}^T\mathbf{T}\mathbf{R}$ and, finally, the following stress resultants are obtained:

$$\begin{aligned} N_1 = \tilde{T}_{11} t = \frac{1}{\lambda_\Theta}\left[\lambda_R \beta_1 + \frac{1}{2}\left({\lambda_R}^3 - \lambda_R\right)\beta_2\right], \\ N_2 = \tilde{T}_{22} t = \frac{1}{\lambda_R}\left[\lambda_\Theta \beta_1 + \frac{1}{2}\left({\lambda_\Theta}^3 - \lambda_\Theta\right)\beta_2\right]. \end{aligned} \tag{23}$$

The derivative of N_1 with respect to φ_R is computed using the chain rule, namely

$$\frac{dN_1}{d\varphi_R} = \frac{\partial N_1}{\partial \lambda_R}\frac{\partial \lambda_R}{\partial \varphi_R} + \frac{\partial N_1}{\partial \lambda_\Theta}\frac{\partial \lambda_\Theta}{\partial \varphi_R}, \tag{24}$$

where

$$\begin{aligned} &\frac{\partial \lambda_R}{\partial \varphi_R} = \frac{\partial \lambda_R}{\partial R}\frac{\partial R}{\partial \varphi_R} = \frac{\lambda_R'}{w}, \\ &\frac{\partial \lambda_\Theta}{\partial \varphi_R} = \frac{\partial \lambda_\Theta}{\partial R}\frac{\partial R}{\partial \varphi_R} = \frac{1}{R} - \frac{\lambda_\Theta}{wR}, \\ &\frac{\partial N_1}{\partial \lambda_R} = \frac{1}{\lambda_\Theta}\left[\beta_1 + \lambda_R \sum_{j=1}^{2}\frac{\partial \beta_1}{\partial I_j}\frac{\partial I_j}{\partial \lambda_R} + \frac{1}{2}\left(3{\lambda_R}^2 - 1\right)\beta_2 + \frac{1}{2}\left({\lambda_R}^3 - \lambda_R\right)\sum_{j=1}^{2}\frac{\partial \beta_2}{\partial I_j}\frac{\partial I_j}{\partial \lambda_R}\right], \\ &\frac{\partial N_1}{\partial \lambda_\Theta} = -\frac{1}{{\lambda_\Theta}^2}\left[\lambda_R \beta_1 + \frac{1}{2}\left({\lambda_R}^3 - \lambda_R\right)\beta_2\right] \end{aligned}$$

$$+\frac{1}{\lambda_\Theta}\left[\lambda_R\sum_{j=1}^{2}\frac{\partial\beta_1}{\partial I_j}\frac{\partial I_j}{\partial\lambda_\Theta}+\frac{1}{2}\left({\lambda_R}^3-\lambda_R\right)\sum_{j=1}^{2}\frac{\partial\beta_2}{\partial I_j}\frac{\partial I_j}{\partial\lambda_\Theta}\right].$$

Introducing (22), (23) and (24) into (21), the equilibrium equations take the following form:

$$\begin{aligned}
\lambda_R' &= \frac{1}{R}\left(\lambda_\Theta\frac{\partial N_1}{\partial\lambda_R}\right)^{-1}\left[\frac{\partial N_1}{\partial\lambda_\Theta}\lambda_\Theta\left(\lambda_\Theta-w\right)-w\left(N_1-N_2\right)\right],\\
\lambda_\Theta' &= \frac{w-\lambda_\Theta}{R},\\
w' &= \frac{w\lambda_R'}{\lambda_R}+\frac{\beta_2\lambda_\Theta^3\left(\lambda_R^2-w^2\right)-2c_2\bar{p}\lambda_\Theta\lambda_R^2\sqrt{\lambda_R^2-w^2}-\lambda_\Theta\left(2\beta_1-\beta_2\right)\left(w^2-\lambda_R^2\right)}{R\lambda_R^2\left(2\beta_1+\beta_2\lambda_R^2-\beta_2\right)},
\end{aligned}\tag{25}$$

with $\bar{p}=pR/c_2$. The system of differential equations (25) is to be solved under the boundary conditions

$$\lambda_R=\lambda_\Theta=w=\lambda_0 \quad \text{at} \quad R=0, \quad \lambda_\Theta=1 \quad \text{at} \quad R=a,$$

with $\lambda_0>1$.

We notice that the form of system (25) remains unchanged if a scaling factor γ is multiplied to R. This invariance property was firstly observed by Yang and Feng [66] when studying the equilibrium problem of circular inflated membranes composed of incompressible Mooney-Rivlin material. This property greatly simplifies the numerical solution. In fact, similarly to the procedure outlined in [66], the solution is obtained as follows: (i) Set the desired value of λ_0; (ii) Set an initial guess value p_0 for pressure p; (iii) Perform the numerical integration of system (25) for increasing values of R, until $\lambda_\Theta=1$. The value of R at which $\lambda_\Theta=1$ is denoted by R_0; (iv) The initial guess p_0 is likely to be different from the correct one and thus R_0 is different from a. However, the invariance property of system (25) allows us to introduce the scaling factor $\gamma=a/R_0$ and compute the correct value of pressure as $\bar{p}=p_0R_0/c_2=p_0a/(\gamma c_2)$. (v) Perform again the numerical integration by setting as initial guess the correct value of $\bar{p}$. From this final integration the stretches profiles are obtained and the deformed shape of the membrane is derived using (20).

The equilibrium equations were written in software MATLAB R2017a. A list of values for λ_0 ranging from 1 to λ_u was defined. According to FE model 1 of Sect. 3, the ultimate stretch considered was $\lambda_u=1.18$. Another list for the initial guess values p_0 was defined. In this regard, the FE pressure-deflection curve of Fig. 5 helped to select reasonable values of p_0. The procedure outlined in the previous paragraph was then carried out for each increasing value of λ_0. The numerical integration of the differential equations was performed using function *ode23t*.

5 Results and Comparison

In this section we compare the results of the approximate analytical solution, the FE analysis and the numerical solution. The numerical solution is based on the assumption that $\lambda_Z=1$ and thus we expect to find good agreement with the analytical solution (14). Same goes for FE model 1, in which transverse contraction is avoided. Instead, FE model 2 takes into account the contraction of the membrane, which means that λ_Z assumes values other than

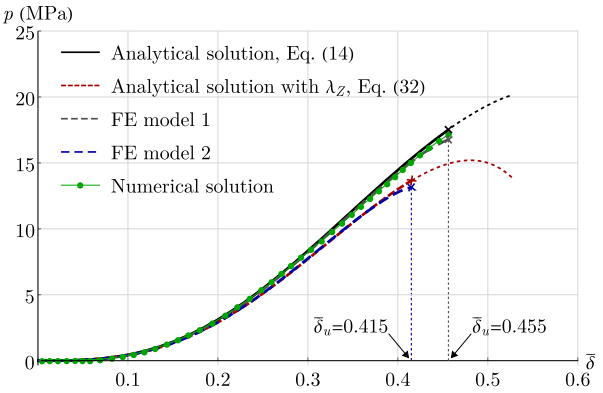

Fig. 7 Pressure-deflection curves with $\bar{\delta} = \delta/a$ of a circular graphene sheet with radius 2.375 μm. Black and red curves represent respectively the analytical solutions without and with transverse contraction. Gray and blue curves are obtained respectively from FE models 1 and 2 while the green curve is the numerical solution

1. Therefore, we expect that the pressure-deflection curve from this model agrees well with the solution proposed in Appendix A, expressed by (32).

We recall that the most plausible assumption is that graphene does not undergo transverse contraction during deformation. Therefore, after the above comparison, we consider only the analytical solution (14) and we compare the pressure-deflection curve with experimental data and numerical simulations from the literature.

5.1 Comparison Between Analytical, FE and Numerical Solutions

The comparison of the pressure-deflection curves obtained from analytical solution, FE simulation and numerical solution is shown in Fig. 7. The ultimate value of stretch considered in the numerical analysis is $\lambda_u = 1.18$, at which ultimate deflection and pressure are respectively $\bar{\delta}_u = 0.455$ and $p_u = 17.10$ MPa. In such configuration, the value of pressure predicted by the analytical solution (14) is 17.27 MPa. The relative error between the two ultimate pressure values is 1.08%. A good match with the simulation of FE model 1 is also observed. In this case, the relative error of the analytical prediction is 2.79%. The good agreement between analytical, FE and numerical solutions demonstrates the accuracy of the formulation proposed in this work.

The profiles of deformation are shown in Fig. 8a. The maximum relative discrepancies of the analytical deformed shapes with respect to the numerical and FE ones are, respectively, 6% and 5.5%. The deformed configurations of the analytical model nearly match the FE ones until $\bar{\delta}$ attains the value 0.4. Then, the membrane in the FE model experienced a higher deformation concentrated in the area close to the center. In fact, Fig. 7 shows that the gap between analytical, numerical and FE pressure-deflection curves becomes more evident after $\bar{\delta} = 0.4$. Nevertheless, we can conclude that the hypothesis of spherical deformed shape provides an accurate description of the kinematics of deformation of the graphene membrane.

The pressure-deflection response from FE model 2 agrees well with the analytical solution with transverse contraction (32). Also in this case, the two pressure-deflection curves nearly match until $\bar{\delta} = 0.4$. The higher discrepancy for $\bar{\delta} > 0.4$ is again explained by observing the comparison of the deformation profiles given in Fig. 8b. The analytical and FE deformed configurations almost coincide for $\bar{\delta} \leq 0.4$, but then the membrane in the FE model experienced a higher deformation in the central area. The value of pressure at $\bar{\delta}_u$ from the analytical solution is 13.65 MPa and the relative error with respect to the FE prediction is 3.96%.

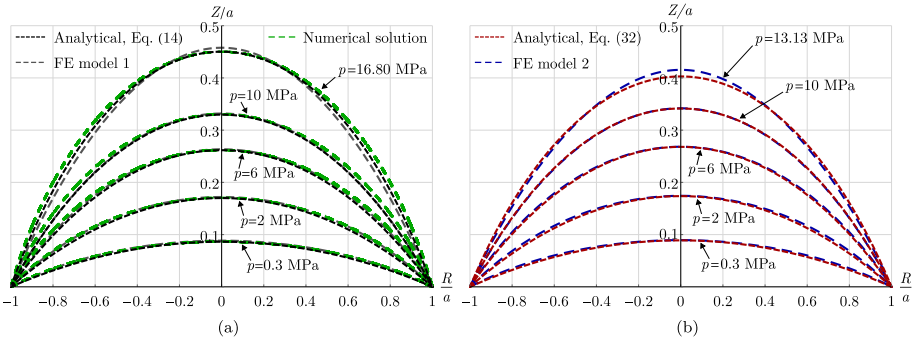

Fig. 8 Profiles of deformation represented in the R-Z plane and given in terms of dimensionless coordinates R/a and Z/a: (**a**) Analytical solution without transverse contraction, numerical solution and FE model 1; (**b**) Analytical solution with transverse contraction and FE model 2

5.2 Comparison with Other Results

We recall that, from a physical point of view, it is doubtful that a one-atom-thick membrane can undergo a transverse contraction. Therefore, the analytical solution that is most consistent with the real response of graphene is the one expressed by (14). From now on, this will be the reference analytical solution and we will compare it with other models, numerical simulations and experiments found in the literature.

The well-known Fichter's model [17] is considered and, for the sake of brevity, it is outlined in Appendix B. The experimental data that we consider are reported in the work by Koenig et al. [29]. In that work, the authors produced monolayer graphene sheets through mechanical exfoliation over predefined microcavities etched in a silica substrate. The microcavities had diameter of around 4.75 μm. A bulge test was performed using a pressure chamber and the deformed shape of the graphene membrane was measured with an atomic force microscope. For the comparison we also consider the FE simulation carried out by Jiang et al. [25]. The FE model was built in software COMSOL Multiphysics using a plate element composed of linearly elastic and isotropic material. The circular plate had diameter of 4.75 μm and it was clamped along the boundary. Geometric nonlinearity was included in the solution.

Figure 9 shows the comparison of the pressure-deflection curves. The black curve (present solution) is expressed by equation (14). The Fichter's solution is in good agreement with our model only for small values of $\bar{\delta}$. This because Fichter's model is based on the assumption of linear elastic material. Such assumption is not suitable for graphene, which exhibits material nonlinearity even for relatively small values of strain [21, 38]. In particular, the uniaxial stress-strain response of graphene shows a progressive reduction of its stiffness until the attainment of the ultimate stress. This is not taken into account in Fichter's model and the result is that, as the strain increases, the gap between its prediction and our solution increases.

From the right side of Fig. 9 we observe a good agreement of our solution with the experimental data by Koenig et al. [29]. However, at some point of the experiment a delamination of graphene from the silica substrate took place. This explains why the last two experimental data (red dots) deviate from the analytical prediction. Very good agreement is found also with the FE simulation of Jiang et al. [25]. Note that their simulation was based on the assumption of linear elastic material. In fact, when $\bar{\delta}$ exceeds 0.12 their prediction becomes slightly stiffer than the response of our model.

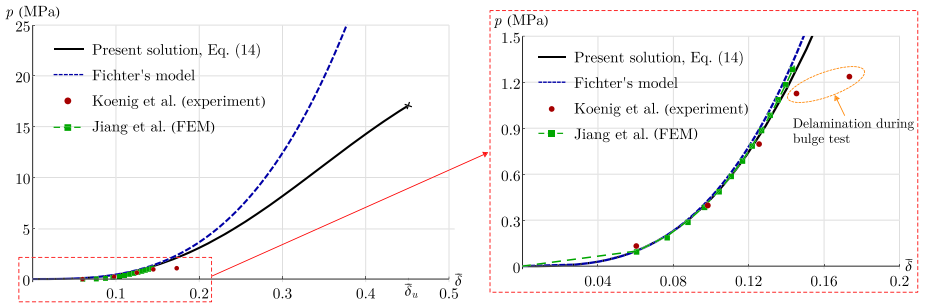

Fig. 9 Comparison of the pressure-deflection curves obtained with the proposed solution (14), Fichter's model [17], experiment from Koenig et al. [29] and FE simulation carried out by Jiang et al. [25] for a graphene membrane with diameter 4.75 μm

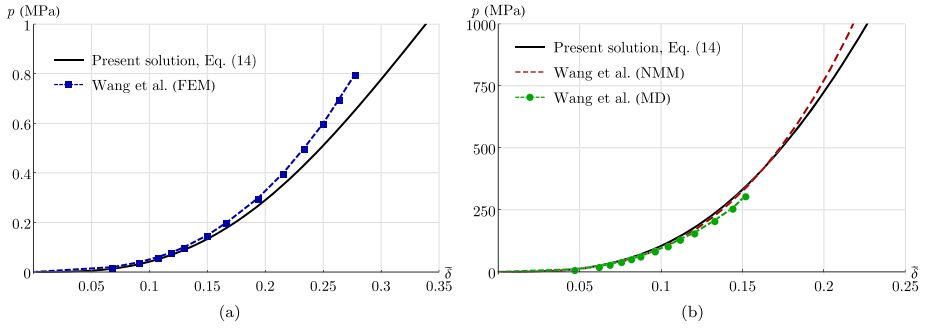

Fig. 10 Comparison with the pressure-deflection curves from (**a**) FE simulation of a graphene sheet with diameter 50 μm, reported in Wang et al. [60], and (**b**) nonlinear membrane model (NMM) and molecular dynamics (MD) simulation of a graphene sheet with diameter 10 nm, reported in Wang et al. [62]

Further comparisons are presented in Fig. 10. In particular, in Fig. 10a we consider the FE simulation carried out by Wang et al. [60] using software ANSYS. The authors used 2-node axisymmetric shell elements composed of a linear elastic material with $E = 1$ TPa and $\nu = 0.17$. As expected, for the same reasons explained previously, the FE simulation matches well with our solution only for relatively small deflections. It is demonstrated once again that the material nonlinearity of graphene plays an important role and must be considered.

Figure 10b shows a comparison with the molecular dynamics (MD) simulation carried out by Wang et al. [62], which is displayed in green color. The graphene membrane had diameter 10 nm. The choice of such a small diameter is due to the fact that MD simulations require a large computational effort and therefore they can be applied only to systems with a relatively small number of atoms. Although the computational strategy is different from the continuum modeling, the simulation is in good agreement with the present solution. The gap is mainly due to the parametrization of the interatomic potential describing the carbon-carbon interactions in graphene. Wang et al. [62] adopted the second-generation reactive empirical bond-order (REBO-2) potential [4], but there are several potentials that can be used and may lead to sensibly different results [19, 20, 42]. The coefficients of the stored energy function (6) adopted in this work were estimated by fitting molecular mechanics simulations based on the modified Morse potential [45].

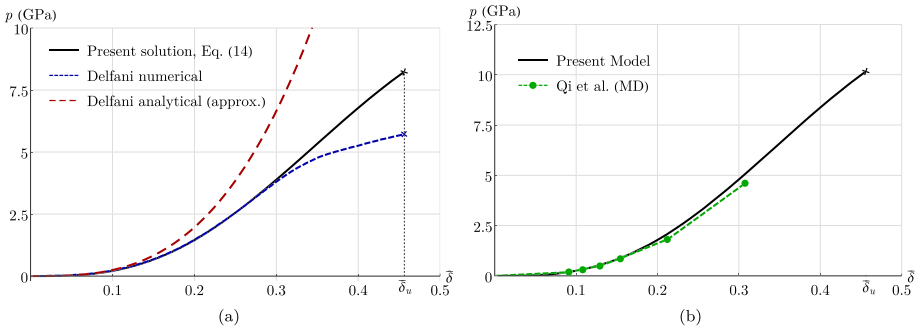

Fig. 11 Comparison with the pressure-deflection curves from (**a**) numerical and approximate analytical solutions by Delfani [14], for a graphene membrane with diameter 10 nm, and (**b**) MD simulation from Qi et al. [52] for a graphene sheet with diameter 8 nm

A nonlinear membrane model (NMM) was also proposed by Wang et al. [62] (equations (3.4) and (3.5) in [62]). The corresponding response of the pressurized graphene membrane is depicted in Fig. 10b. We observe again a good match with our analytical prediction for relatively small deflections. The model proposed in [62] does not take into account material nonlinearity and thus it deviates from our solution as the deflection increases.

The comparison with the experimental data by Koenig et al. [29] showed that delamination of graphene from a silica substrate takes place for relatively small deformations. In such case, as visible in Fig. 9, an accurate prediction is obtained even with a model in linear elasticity. However, nowadays there are more and more studies where suspended monolayer and multilayer graphene films are produced and employed for mechanical, optical and electronic sensors. For instance, Afyouni et al. [2] produced graphene through chemical vapor deposition and then removed the substrate obtaining clean graphene membranes with diameter up to 750 μm. Other examples can be found in [3, 8, 12]. Being not connected to a substrate, suspended graphene does not experience delamination and therefore it can undergo large deformations. In this case, nonlinear formulations such as the one proposed in this work are required.

To this regard, very few authors analyzed the problem of pressurized graphene membranes in nonlinear elasticity. A recent solution was proposed by Delfani [14]. He considered the nonlinear constitutive model proposed in [15] and derived the equilibrium equations of the thin plate theory in absence of body forces. Consequently, he presented an application to the case of a circular graphene sheet subjected to bulge test. Due to the complexity of the equilibrium equations, he proposed a numerical solution by expanding in series the unknown displacement components. The series were truncated at the fifth order in parameter $q = p/E$. He also proposed an approximate analytical solution valid for small deflections, which is reported in equation (89) of [14].

In Fig. 11a, we compare the solution proposed in the present work with the numerical and analytical ones proposed by Delfani. We observe that the present solution matches the numerical one proposed by Delfani until relatively large deformations ($\bar{\delta} \leq 0.3$), then the two solutions diverge. This because the numerical solution by Delfani was obtained with a truncation at the fifth order in q, which results in a loss of accuracy for large deflections ($\bar{\delta} > 0.3$). As expected, due to the mathematical simplifications performed thanks to the hypothesis of small deflections, the approximate analytical solution by Delfani matches the present solution only for small values of $\bar{\delta}$.

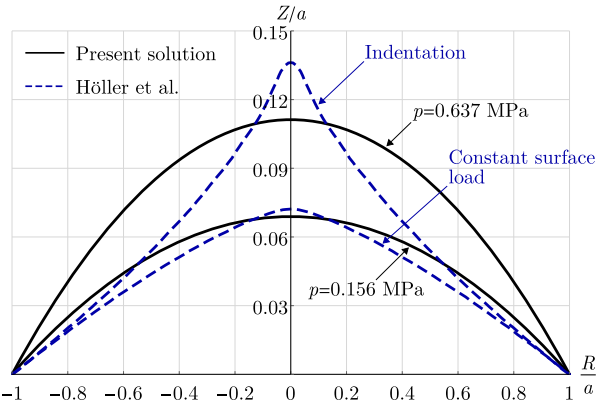

Fig. 12 Comparison between profiles of deformation of graphene under uniform lateral pressure (present solution), constant surface load and indentation (results from Höller et al. [22]). The values of pressure applied on the membrane are such that the resultants of the external forces match those considered in [22]

Another nonlinear simulation of pressurized graphene was presented by Qi et al. [52]. The authors carried out MD simulations adopting the AIREBO potential to describe the carbon-carbon interactions. They considered a circular graphene membrane with radius 4 nm. In the work [52], the authors reported the pressure-deflection response until a value of deflection $\bar{\delta} \approx 0.31$. From Fig. 11b, we observe that their prediction agrees quite well with the analytical formula proposed in this work. The gap between the two curves reaches a maximum of 9% and it is mostly due to the different interatomic potentials adopted. We recall that atomistic simulations require a large computational effort, thus they are suitable only for very small systems. On the other hand, the present analytical solution is particularly advantageous from this point of view.

5.3 Response Under Different Lateral Loads

In order to show the variations in the response of graphene under different lateral loads, Fig. 12 depicts the profiles of deformation under constant surface load and indentation. The results are obtained from the work by Höller et al. [22]. In particular, the authors reported the cases of a constant surface load and a load concentrated in the center of the membrane. In the first case, the surface load applied to the membrane was 0.156 MPa. In the second case, a lateral force equal to 500 nN was applied. To compare the shapes of the deformed graphene membrane with the case of uniform lateral pressure, the deformed profiles from the present solution are shown in Fig. 12. The values of pressure considered are such that the resultants of the external loads match with those applied in [22]. Note that, in this comparison, the results are obtained using the constitutive parameters given in [22].

6 Membranes Composed of Graphene Deposited onto a Soft Surface

Many applications in nanotechnologies involve the use of layered nanocomposites formed by graphene deposited onto a substrate. In general, when a layered nanocomposite is subjected to lateral pressure there is no delamination. Therefore, the capability of graphene to undergo large deformations can be exploited and material nonlinearity plays a role in the mechanical response. In the present section we use the analytical solution (14) to predict the pressure-deflection response of a graphene nanocomposite.

We consider a two-layered composite membrane formed by graphene deposited onto a soft substrate. The membrane is circular with radius a and the thickness of the substrate is

h. We recall that we assume a graphene thickness $t = 0.335$ nm and we introduce $\eta = t/h$, which expresses the volume fraction of graphene.

A compressible Mooney-Rivlin material model is adopted for the soft substrate, which is defined by the stored energy function

$$\omega(I_1, I_2, I_3) = C_1(\imath_1 - 3) + C_2(\imath_2 - 3) + C_3(\imath_3 - 1) - (C_1 + 2C_2 + C_3)\ln \imath_3,$$

where constitutive parameters C_1, C_2 and C_3 have dimension or force per unit area. Under the hypothesis of spherical deformed shape, the radial Cauchy stress T_0^S of the substrate when $R \to 0$ reads [46]

$$T_0^S = \frac{2\sin^2\psi_0\left(\psi_0^2\csc^2\psi_0 - 1\right)\left(C_1 + C_2\,\psi_0^2\csc^2\psi_0\right)\left[C_1 + 2C_2 + \psi_0^2\csc^2\psi_0(2C_2 + C_3) + C_3\left(1 + \psi_0^4\csc^4\psi_0\right)\right]}{\psi_0^2\sqrt{(C_1 + 2C_2 + C_3)\left(C_1 + 2C_2\,\psi_0^2\csc^2\psi_0 + C_3\,\psi_0^4\csc^4\psi_0\right)}}.$$

The principal Cauchy radial stress T_0^G of the graphene sheet is expressed by (12).

We assume a uniform strain distribution between graphene and substrate (isostrain). This assumption has been widely used for predicting the elastic properties of layered composites [26]. The prediction is especially accurate when there is a strong bond between the layers and the thickness of each layer is much smaller than the other two dimensions [35]. Under isostrain state, the equilibrium equation (13) in case of composite membrane becomes

$$p = \frac{2h\left(\eta\, T_0^G + T_0^S\right)}{\rho}, \tag{26}$$

where $\rho = a/\sin\psi_0$. The expression of pressure p is written as function of the normalized deflection using $\psi_0 = 2\arctan\bar{\delta}$, with $\bar{\delta} = \delta/a$.

In order to show the effect of graphene in a composite membrane of practical interest, we consider a silicone substrate characterized by the constitutive parameters given in Table 4 of work [46]. For nanocomposites made of monolayer graphene deposited on a substrate, the typical volume fraction of graphene ranges from 10^{-6} to 10^{-4}. The pressure-deflection response for several values of η in such range is displayed in Fig. 13a, where $\bar{p} = pa/(C_1 h)$. The ultimate deflection considered is $\bar{\delta}_u = 0.455$, as reported in Sect. 5.1. We observe that small volume fractions of graphene have a remarkable impact on the final response of the nanocomposite, which becomes much stiffer compared to that of the bare substrate.

In the following, an expression of the equivalent Young's modulus of the composite membrane is derived. We introduce into (26) the linearized form of the radial Cauchy stress, expressed by (17), for both substrate and graphene contributions. The following linearized expression of the applied pressure is derived:

$$p = \left[\eta\frac{E_G}{(1-\nu_G)} + \frac{E_S}{(1-\nu_S)}\right]\frac{8h}{3a}\arctan^3\bar{\delta}.$$

The equivalent Young's modulus E_C is computed by equating the above expression of p with the one in (19), valid for a membrane of homogeneous material. Note that, in this case, equation (19) is computed with the thickness of the composite membrane, namely $h(1+\eta)$. The following expression for E_C is obtained:

$$E_C = \left[\eta\frac{E_G}{(1-\nu_G)} + \frac{E_S}{(1-\nu_S)}\right]\frac{(1-\nu_C)}{(1+\eta)}.$$

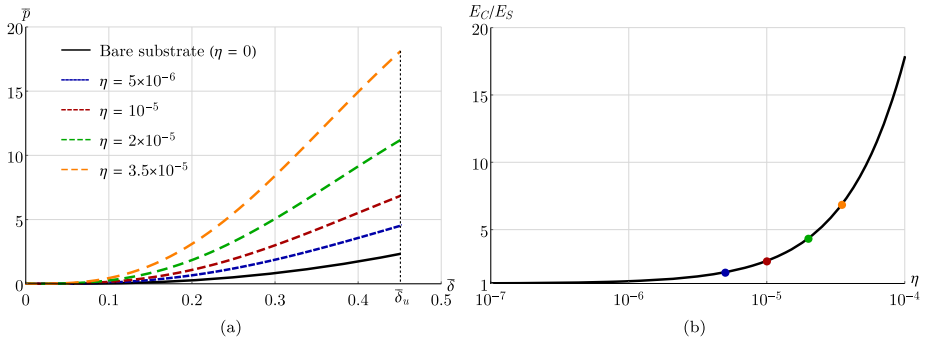

Fig. 13 Two-layered composite membrane made of graphene deposited on a silicone substrate: (**a**) Pressure-deflection curves from (26) for increasing volume fractions of graphene, expressed by $\eta = t/h$, with t and h indicating respectively graphene and substrate thicknesses; (**b**) Semi-logarithmic plot of the ratio between Young's moduli of composite membrane and bare substrate, E_C/E_S, as a function of the graphene volume fraction η

As previously mentioned, the volume fraction of graphene in most layered nanocomposites ranges from 10^{-6} to 10^{-4}. Thus we expect that the presence of graphene has a negligible effect on the Poisson's ratio ν_C of the nanocomposite ($\nu_C \approx \nu_S$). Under this assumption, the expression of E_C becomes

$$E_C = \frac{\eta E_G\,(1-\nu_S) + E_S\,(1-\nu_G)}{(1+\eta)\,(1-\nu_G)}.$$

The Young's modulus E_S and Poisson's ratio ν_S of the silicone substrate analyzed previously are computed using equation (24) of work [46]. The elastic constants of graphene are computed using (18), obtaining $E = 1042.9$ GPa and $\nu = 0.146$. A plot of the ratio between Young's moduli of composite membrane and bare substrate with increasing volume fractions of graphene is shown in Fig. 13b.

7 Conclusions

In the present work we analyzed the problem of circular graphene membranes subjected to uniform lateral pressure. The analytical formulation was developed in finite elasticity. The kinematics of deformation was described by assuming that the membrane preserves the axisymmetry and deforms into a spherical cap. The material behavior was described by a hyperelastic stored energy function that takes into account both nonlinearity and anisotropy of graphene. Assuming that the graphene membrane does not experience transverse contraction and writing the equilibrium for $R \to 0$, an approximate solution expressing the applied pressure as a function of the deflection was derived. In addition, another solution considering the transverse contraction was proposed in Appendix A. This solution may be a good basis for modeling membranes composed of multilayer graphene, where transverse contraction should be considered.

A FE analysis was carried out in COMSOL using the 3D membrane interface. Both material nonlinearity and anisotropy of graphene were included. It was shown that for circular pressurized graphene membranes the effect of material anisotropy is negligible and thus the

deformed configuration remains axisymmetric. Furthermore, it was verified that a spherical cap provides an accurate description of the kinematics of deformation.

To provide a comprehensive investigation of the mechanics of pressurized graphene membranes, a numerical solution of the equilibrium problem of the exact theory was proposed. The simplifying hypothesis on the kinematics of the analytical model was abandoned. The differential equilibrium equations were derived and solved with a numerical procedure implemented in MATLAB. The results from FE, numerical and analytical solutions agree well, demonstrating that the proposed formulation is accurate.

A comparison with other models, numerical simulations and experiments found in the literature was presented. Good agreement in the pressure-deflection curves was found for relatively small deflections. However, in most cases, significant differences were observed for large deflections. This because, differently from our entirely nonlinear approach, most continuum models in the literature are based on the assumption of linear elastic material. The comparison with the numerical solution in nonlinear elasticity proposed by Delfani [14] showed good agreement even for deflections that go well beyond the range of application of the linearized theory. Nevertheless, in addition to being a numerical approach, the above solution loses accuracy for $\bar{\delta} > 0.3$. The foregoing considerations point out the novelty of the present work and the importance of considering the nonlinear material response of graphene.

The proposed analytical solution was then employed to study the pressure-deflection behavior of a two-layered membrane made of graphene deposited onto a soft substrate. The effect of graphene on the final response was investigated and the equivalent Young's modulus of the nanocomposite was derived. This application may be important because nowadays nanotechnologies often involve layered nanocomposites.

The approximate solution proposed in this work is a useful tool for accurate predictions of the response of pressurized graphene membranes. For the first time, a pressure-deflection relation in nonlinear elasticity was proposed. This is a great advantage in terms of applicability because it does not require any computational effort, which is the main concern in atomistic and FE simulations.

Appendix A: Analytical Solution with Transverse Contraction

After deformation, thickness t transforms into $t' = \lambda_Z t$ and the deformation gradient reads [46]

$$[\mathbf{F}] = \begin{bmatrix} \rho \dfrac{\partial \psi}{\partial R} \cos\psi & 0 & \lambda_Z \sin\psi \\ 0 & \dfrac{\rho \sin\psi}{R} & 0 \\ -\rho \dfrac{\partial \psi}{\partial R} \sin\psi & 0 & \lambda_Z \cos\psi \end{bmatrix}.$$

Rotation tensor $\mathbf{R}$ remains unchanged and right stretch tensor $\mathbf{U}$ becomes

$$[\mathbf{U}] = \begin{bmatrix} \rho \dfrac{\partial \psi}{\partial R} & 0 & 0 \\ 0 & \dfrac{\rho \sin\psi}{R} & 0 \\ 0 & 0 & \lambda_Z \end{bmatrix}.$$

The right Cauchy-Green deformation tensor and the Green-Lagrange strain tensor expressed in cylindrical coordinates assume the form

$$[\mathbf{C}] = \begin{bmatrix} \lambda_R^2 & 0 & 0 \\ 0 & \lambda_\Theta^2 & 0 \\ 0 & 0 & \lambda_Z^2 \end{bmatrix}, \qquad [\mathbf{E}] = \frac{1}{2}\begin{bmatrix} \lambda_R^2 - 1 & 0 & 0 \\ 0 & \lambda_\Theta^2 - 1 & 0 \\ 0 & 0 & \lambda_Z^2 - 1 \end{bmatrix},$$

where λ_R and λ_Θ are given by (2).

Strain invariants I_1 and I_2 become

$$\begin{aligned} I_1 &= \frac{1}{2}\left(\lambda_R^2 + \lambda_\Theta^2 + \lambda_Z^2 - 3\right), \\ I_2 &= \frac{1}{4}\left(\lambda_R^2 - 1\right)\left(\lambda_\Theta^2 - 1\right) + \frac{1}{4}\left(\lambda_R^2 - 1\right)\left(\lambda_Z^2 - 1\right) + \frac{1}{4}\left(\lambda_\Theta^2 - 1\right)\left(\lambda_Z^2 - 1\right), \end{aligned} \tag{27}$$

while invariant I_3 has the same expression as in (5). The second Piola-Kirchhoff stress tensor is computed using (7), obtaining

$$\begin{aligned} \Sigma_{RR} &= \frac{\beta_1}{t} + \frac{\beta_2}{2t}\left(\lambda_R^2 - 1\right) + \frac{3\beta_3}{4t}\left(\lambda_R^2 - \lambda_\Theta^2\right)^2 \cos(6\phi), \\ \Sigma_{\Theta\Theta} &= \frac{\beta_1}{t} + \frac{\beta_2}{2t}\left(\lambda_\Theta^2 - 1\right) - \frac{3\beta_3}{4t}\left(\lambda_R^2 - \lambda_\Theta^2\right)^2 \cos(6\phi), \\ \Sigma_{ZZ} &= \frac{\beta_1}{t} + \frac{\beta_2}{2t}\left(\lambda_Z^2 - 1\right), \\ \Sigma_{R\Theta} &= -\frac{3\beta_3}{4t}\left(\lambda_R^2 - \lambda_\Theta^2\right)^2 \sin(6\phi), \quad \Sigma_{RZ} = \Sigma_{\Theta Z} = 0, \end{aligned} \tag{28}$$

where β_1, β_2 and β_3 are given in (8). The first Piola-Kirchhoff stress tensor is thus derived

$$[\mathbf{T}_R] = \begin{bmatrix} \lambda_R \Sigma_{RR} \cos\psi & \lambda_R \Sigma_{R\Theta} \cos\psi & \lambda_Z \Sigma_{ZZ} \sin\psi \\ \lambda_\Theta \Sigma_{R\Theta} & \lambda_\Theta \Sigma_{\Theta\Theta} & 0 \\ -\lambda_R \Sigma_{RR} \sin\psi & -\lambda_R \Sigma_{R\Theta} \sin\psi & \lambda_Z \Sigma_{ZZ} \cos\psi \end{bmatrix}.$$

Condition $\mathbf{T}_R \mathbf{n}_Z = \mathbf{0}$ for the membrane stress state requires that

$$\lambda_Z \Sigma_{ZZ} \sin\psi = 0 \quad \text{and} \quad \lambda_Z \Sigma_{ZZ} \cos\psi = 0, \quad \forall \psi \in [0, \pi/6], \tag{29}$$

which are satisfied only if $\Sigma_{ZZ} = 0$. From this condition and recalling (28), we derive the following implicit expression of stretch λ_Z:

$$\lambda_Z = \sqrt{1 - 2\frac{\beta_1}{\beta_2}}. \tag{30}$$

Finally, the components of the Cauchy stress tensor read

$$\begin{aligned} T_{RR} &= \frac{\lambda_R}{\lambda_\Theta \lambda_Z} \Sigma_{RR} \cos^2\psi, & T_{\Theta\Theta} &= \frac{\lambda_\Theta}{\lambda_R \lambda_Z} \Sigma_{\Theta\Theta}, & T_{ZZ} &= \frac{\lambda_R}{\lambda_\Theta \lambda_Z} \Sigma_{RR} \sin^2\psi, \\ T_{R\Theta} &= \frac{1}{\lambda_Z} \Sigma_{R\Theta} \cos\psi, & T_{RZ} &= -\frac{\lambda_R}{\lambda_\Theta \lambda_Z} \Sigma_{RR} \cos\psi \sin\psi, & T_{\Theta Z} &= -\frac{1}{\lambda_Z} \Sigma_{R\Theta} \sin\psi, \end{aligned}$$

with λ_Z expressed by (30).

As we did in Sect. 2, we now write the equilibrium in the neighborhood of the central point of the membrane. With this aim, we firstly compute the Cauchy stress tensor for the limit case of $R \to 0$. Radial and circumferential stretches are equal to each other ($\lambda_R = \lambda_\Theta|_{R\to 0} = \lambda$) and third invariant I_3 goes to zero. The only non-zero components of the Cauchy stress tensor are

$$T_{RR}|_{R\to 0} = T_{\Theta\Theta}|_{R\to 0} = T_0 = \frac{\psi_0^2 \csc \psi_0^2 - \lambda_Z^2\big|_{R\to 0}}{2t\ \lambda_Z|_{R\to 0}}\ \beta_2|_{R\to 0}\,. \tag{31}$$

Hereinafter, for the sake of simplicity, we indicate $\lambda_Z|_{R\to 0}$ simply with λ_Z. Equilibrium equation (13) becomes

$$p = \frac{2T_0\lambda_Z t}{\rho},$$

from which, using (31), (8) and (27), we derive the following expression of the applied pressure:

$$p = \frac{\sin\psi_0}{8a}\left(\psi_0^2 \csc^2\psi_0 - \lambda_Z^2\right)\sum_{j=0}^{3}\zeta_j\,\psi_0^{2j}\csc^{2j}\psi_0, \tag{32}$$

where

$$\begin{aligned}
\zeta_0 &= \lambda_Z^2\left[\lambda_Z^2\left(5c_{10}\lambda_Z^2 - c_{11}\lambda_Z^2 - 25c_{10} - 3c_{11} + 4c_{12}\right) + 8c_7\left(\lambda_Z^2 - 4\right) - 2c_9\left(\lambda_Z^2 + 2\right)\right.\\
&\quad \left. - 4c_6 + 8c_8 + 9\left(5c_{10} + 3c_{11} - 2c_{12}\right)\right]\\
&\quad + 12c_5\left(\lambda_Z^2 - 3\right) - 8c_2 + 16c_4 + 3\left(4c_6 + 16c_7 - 4c_8 + 2c_9 - 15c_{10} - 9c_{11} + 6c_{12}\right),\\
\zeta_1 &= 2\lambda_Z^2\left[3c_{11}\left(\lambda_Z^2 - 8\right) - 2c_{12}\left(\lambda_Z^2 - 7\right) + 5c_{10}\left(\lambda_Z^2 - 4\right) - 4c_8 + 4c_9\right] + 16c_7\left(\lambda_Z^2 - 4\right)\\
&\quad + 24c_5 - 8c_6 + 16c_8 - 8c_9 + 90c_{10} + 54c_{11} - 36c_{12},\\
\zeta_2 &= 2\left[c_{12}\left(11 - 5\lambda_Z^2\right) + 5c_{10}\left(\lambda_Z^2 - 7\right) + 3c_{11}\left(3\lambda_Z^2 - 5\right) + 12c_7 - 2c_8\right],\\
\zeta_3 &= 4\left(5c_{10} + c_{11} - c_{12}\right).
\end{aligned}$$

An explicit expression of stretch λ_Z is derived by satisfying condition (29) for the limit case of $R \to 0$, for which $\lambda_R = \lambda_\Theta|_{R\to 0} = \lambda$. In this case, substitution of (8) and (27) into (30) gives

$$\sqrt{\eta} - \sqrt{\frac{\Delta_n}{\Delta_d}} = 0, \tag{33}$$

with $\eta = \lambda_Z^2$ and

$$\begin{aligned}
\Delta_n = &-8c_2\left(\eta + 2\lambda^2 - 2\right) + 16c_4 + 12c_5\left[-\eta + 2\left(\eta - 1\right)\lambda^2 + \lambda^4\right]\\
&- 4c_6\left[\eta^2 - 7\eta + 2\left(3\eta - 7\right)\lambda^2 + 5\lambda^4 + 9\right]\\
&+ 8c_7\left[-\eta^2 + 5\eta + \left(5\eta - 8\right)\lambda^4 + 2\left(\eta - 5\right)\left(\eta - 1\right)\lambda^2 + 2\lambda^6 - 3\right]\\
&- 4c_8\left(\lambda - 1\right)\left(\lambda + 1\right)\left(2\eta + \lambda^2 - 3\right)\left(\eta + 2\lambda^2 - 2\right)
\end{aligned}$$

$$
\begin{aligned}
&- 2c_9\left[\eta^3 - 4\eta^2 + 11\eta + 2(\eta-7)\lambda^4 + 2\left(\eta^2 - 6\eta + 11\right)\lambda^2 + 4\lambda^6 - 12\right] \\
&+ 5c_{10}\left\{-\eta^3 + 6\eta^2 - 15\eta + 8(\eta-2)\lambda^6 + [\eta(5\eta - 32) + 33]\lambda^4\right. \\
&\left.+ 2(\eta-1)[(\eta-6)\eta + 15]\lambda^2 + 3\lambda^8 + 9\right\} \\
&- c_{11}\left\{\eta\left[(\eta-5)\eta^2 + 9\right] + 8(1-2\eta)\lambda^6 - 3[5(\eta-4)\eta + 9]\lambda^4\right. \\
&\left.+ 2\left[\eta\left(\eta^2 + 9\eta - 27\right) + 9\right]\lambda^2 + \lambda^8\right\} \\
&- c_{12}(\lambda-1)(\lambda+1)\left(2\eta + \lambda^2 - 3\right)\left[2(\eta-6)\eta + 10\eta\lambda^2 + 9\lambda^4 - 24\lambda^2 + 15\right], \\
\Delta_d = &- 8c_2 + 16c_4 + 12c_5\left(\eta + 2\lambda^2 - 3\right) - 4c_6\left(\eta + 2\lambda^2 - 3\right) \\
&+ 8c_7\left[\eta^2 + 2(\eta-4)\lambda^2 - 4\eta + 3\lambda^4 + 6\right] \\
&- 4c_8\left(\lambda^2 - 1\right)\left(2\eta + \lambda^2 - 3\right) - 2c_9(\eta-1)\left(\eta - 4\lambda^2 + 3\right) \\
&+ 5c_{10}\left(\eta + 2\lambda^2 - 3\right)\left[(\eta-2)\eta + 2\lambda^4 - 4\lambda^2 + 3\right] \\
&- c_{11}\left(\eta + 2\lambda^2 - 3\right)\left[\eta^2 + 4(3-2\eta)\lambda^2 + 6\eta - 2\lambda^4 - 9\right] \\
&- 2c_{12}(\lambda-1)(\lambda+1)\left(2\eta + \lambda^2 - 3\right)\left(\eta + 2\lambda^2 - 3\right).
\end{aligned}
$$

Equation (33) admits four solutions in η. Two solutions are not real and another one does not respect condition $\eta = 1$ when $\lambda = 1$. The remaining solution is the correct one. We do not report this solution due to its very long mathematical expression. Having obtained an explicit expression for η, we compute $\lambda_Z = \sqrt{\eta}$ and by substitution into (32) we finally derive the pressure-deflection equation. We recall that relation $\psi_0 = 2\arctan\bar{\delta}$ allows us to obtain a direct expression of pressure as a function of deflection.

Appendix B: Fichter's Model

Fichter's model is based on the assumption that the material is linearly elastic. In this case, the equilibrium equations are

$$
\begin{aligned}
&N^2\left(\bar{R}^2\frac{d^2N}{d\bar{R}^2} + 3\bar{R}\frac{dN}{d\bar{R}}\right) - \frac{1}{2}\bar{R}^3\frac{dN}{d\bar{R}} + \frac{1}{2}(3+\nu)\bar{R}^2N + \frac{1}{4}\frac{\bar{R}^2EH}{pL} = 0, \\
&N\frac{d\bar{\delta}}{d\bar{R}} + \frac{1}{2}\bar{R} = 0,
\end{aligned}
\tag{34}
$$

where $\bar{R} = R/a$, E is the Young's modulus, ν is the Poisson's ratio and $N = N_R/(pa)$, with N_R indicating the radial stress resultant. Young's modulus and Poisson's ratio of graphene are computed using (18), obtaining $E = 1042.9$ GPa and $\nu = 0.146$. The solution for both stress resultant and deflection is found in the form of a power series

$$
\begin{aligned}
N\left(\bar{R}\right) &= \sum_0^\infty n_{2m}\bar{R}^{2m}, \\
\bar{\delta}\left(\bar{R}\right) &= \sum_0^\infty w_{2n}\left(1 - \bar{R}^{2n+2}\right).
\end{aligned}
\tag{35}
$$

Substituting $(35)_1$ into $(34)_1$ and equating coefficients of like powers of $\bar{R}$ we obtain a system of equations that allows to derive the expressions of coefficients n_{2m} as functions of n_0. Likewise, substituting $(35)_2$ into $(34)_2$ and equating coefficients of like powers of $\bar{R}$ we derive the expressions of coefficients w_{2n} as functions of n_0. Finally, n_0 is evaluated by imposing the following boundary condition on radial displacement:

$$\left\{\bar{R}\left[\frac{d}{d\bar{R}}\left(\bar{R}N\right)-\nu N-\bar{R}\frac{d\bar{\delta}}{d\bar{R}}\right]\right\}\Bigg|_{\bar{R}=1}=0.$$

This procedure was implemented in software Wolfram Mathematica. A vector of increasing pressure values was defined and, for each value, the solution was obtained by considering twelve terms in the power series ($m = 12$ and $n = 12$). More terms did not cause sensible variations in the solutions and only increased the computational burden.

Acknowledgements This work was supported by the Italian Ministry of University and Research (MUR) through research grant PRIN 2020 No. 2020EBLPLS on "Opportunities and challenges of nanotechnology in advanced and green construction materials" and through project FISR 2019 "Eco Earth" (code 00245). Financial support by the National Group of Mathematical Physics (GNFM-INdAM) is also acknowledged.

Declarations

Competing Interests The authors declare that they have no conflict of interest.

References

1. Adkins, J.E., Rivlin, R.S.: Large elastic deformations of isotropic materials IX. The deformation of thin shells. Philos. Trans. R. Soc. Lond. Ser. A, Math. Phys. Sci. **244**(888), 505–531 (1952)
2. Afyouni Akbari, S., Ghafarinia, V., Larsen, T., Parmar, M.M., Villanueva, L.G.: Large suspended monolayer and bilayer graphene membranes with diameter up to 750 μm. Sci. Rep. **10**(1), 1–8 (2020)
3. Alemán, B., Regan, W., Aloni, S., Altoe, V., Alem, N., Girit, C., Geng, B., Maserati, L., Crommie, M., Wang, F., et al.: Transfer-free batch fabrication of large-area suspended graphene membranes. ACS Nano **4**(8), 4762–4768 (2010)
4. Brenner, D.W., Shenderova, O.A., Harrison, J.A., Stuart, S.J., Ni, B., Sinnott, S.B.: A second-generation reactive empirical bond order (REBO) potential energy expression for hydrocarbons. J. Phys. Condens. Matter **14**(4), 783 (2002)
5. Bunch, J.S., Verbridge, S.S., Alden, J.S., Van Der Zande, A.M., Parpia, J.M., Craighead, H.G., McEuen, P.L.: Impermeable atomic membranes from graphene sheets. Nano Lett. **8**(8), 2458–2462 (2008)
6. Caillerie, D., Mourad, A., Raoult, A.: Discrete homogenization in graphene sheet modeling. J. Elast. **84**(1), 33–68 (2006)
7. Cao, C., Daly, M., Singh, C.V., Sun, Y., Filleter, T.: High strength measurement of monolayer graphene oxide. Carbon **81**, 497–504 (2015)
8. Carvalho, A.F., Fernandes, A.J., Hassine, M.B., Ferreira, P., Fortunato, E., Costa, F.M.: Millimeter-sized few-layer suspended graphene membranes. Appl. Mater. Today **21**, 100879 (2020)
9. Casey, J.: On infinitesimal deformation measures. J. Elast. **28**(3), 257–269 (1992)
10. Chae, S.H., Lee, Y.H.: Carbon nanotubes and graphene towards soft electronics. Nano Converg. **1**(1), 1–26 (2014)
11. Chen, M., Haddon, R.C., Yan, R., Bekyarova, E.: Advances in transferring chemical vapour deposition graphene: a review. Mater. Horiz. **4**(6), 1054–1063 (2017)
12. Chen, Y.M., He, S.M., Huang, C.H., Huang, C.C., Shih, W.P., Chu, C.L., Kong, J., Li, J., Su, C.Y.: Ultra-large suspended graphene as a highly elastic membrane for capacitive pressure sensors. Nanoscale **8**(6), 3555–3564 (2016)
13. Chun, S., Kim, Y., Oh, H.S., Bae, G., Park, W.: A highly sensitive pressure sensor using a double-layered graphene structure for tactile sensing. Nanoscale **7**(27), 11652–11659 (2015)
14. Delfani, M.R.: Nonlinear elasticity of monolayer hexagonal crystals: Theory and application to circular bulge test. Eur. J. Mech. A, Solids **68**, 117–132 (2018)

15. Delfani, M.R., Shodja, H.M., Ojaghnezhad, F.: Mechanics and morphology of single-walled carbon nanotubes: from graphene to the elastica. Philos. Mag. **93**(17), 2057–2088 (2013)
16. Fang, M., Wang, K., Lu, H., Yang, Y., Nutt, S.: Covalent polymer functionalization of graphene nanosheets and mechanical properties of composites. J. Mater. Chem. **19**(38), 7098–7105 (2009)
17. Fichter, W.B.: Some solutions for the large deflections of uniformly loaded circular membranes, vol. 3658. National Aeronautics and Space Administration, Langley Research Center (1997). https://ntrs.nasa.gov/citations/19970023537
18. Freddi, F., Royer-Carfagni, G.: From non-linear elasticity to linearized theory: examples defying intuition. J. Elast. **96**(1), 1–26 (2009)
19. Genoese, A., Genoese, A., Rizzi, N.L., Salerno, G.: On the derivation of the elastic properties of lattice nanostructures: the case of graphene sheets. Composites, Part B, Eng. **115**, 316–329 (2017)
20. Genoese, A., Genoese, A., Salerno, G.: In-plane and out-of-plane tensile behaviour of single-layer graphene sheets: a new interatomic potential. Acta Mech. **231**(7), 2915–2930 (2020)
21. Georgantzinos, S.K., Katsareas, D.E., Anifantis, N.K.: Graphene characterization: A fully non-linear spring-based finite element prediction. Physica E, Low-Dimens. Syst. Nanostruct. **43**(10), 1833–1839 (2011)
22. Höller, R., Libisch, F., Hellmich, C.: A membrane theory for circular graphene sheets, based on a hyperelastic material model for large deformations. Mech. Adv. Mat. Struct. **29**(5), 651–661 (2022)
23. Höller, R., Smejkal, V., Libisch, F., Hellmich, C.: Energy landscapes of graphene under general deformations: DFT-to-hyperelasticity upscaling. Int. J. Eng. Sci. **154**, 103342 (2020)
24. Hossain, M.Z., Ahmed, T., Silverman, B., Khawaja, M.S., Calderon, J., Rutten, A., Tse, S.: Anisotropic toughness and strength in graphene and its atomistic origin. J. Mech. Phys. Solids **110**, 118–136 (2018)
25. Jiang, S., Shi, S., Wang, X.: Nanomechanics and vibration analysis of graphene sheets via a 2D plate model. J. Phys. D, Appl. Phys. **47**(4), 045104 (2013)
26. Kalidindi, S.R., Franco, E.: Numerical evaluation of isostrain and weighted-average models for elastic moduli of three-dimensional composites. Compos. Sci. Technol. **57**(3), 293–305 (1997)
27. Kang, X., Wang, J., Wu, H., Liu, J., Aksay, I.A., Lin, Y.: A graphene-based electrochemical sensor for sensitive detection of paracetamol. Talanta **81**(3), 754–759 (2010)
28. Kausar, A.: Applications of polymer/graphene nanocomposite membranes: a review. Mater. Res. Innov. **23**(5), 276–287 (2019)
29. Koenig, S.P., Boddeti, N.G., Dunn, M.L., Bunch, J.S.: Ultrastrong adhesion of graphene membranes. Nat. Nanotechnol. **6**(9), 543–546 (2011)
30. Korobeynikov, S.N., Alyokhin, V.V., Babichev, A.V.: On the molecular mechanics of single layer graphene sheets. Int. J. Eng. Sci. **133**, 109–131 (2018)
31. Kumar, S., Parks, D.M.: On the hyperelastic softening and elastic instabilities in graphene. Proc. R. Soc. A, Math. Phys. Eng. Sci. **471**(2173), 20140567 (2015)
32. Lee, C., Wei, X., Kysar, J.W., Hone, J.: Measurement of the elastic properties and intrinsic strength of monolayer graphene. Science **321**(5887), 385–388 (2008)
33. Li, C., Xiao, J., Guo, T., Fan, S., Jin, W.: Effects of graphene membrane parameters on diaphragm-type optical fibre pressure sensing characteristics. Mater. Res. Innov. **19**(sup5), S5–17 (2015)
34. Lin, W.H., Chen, T.H., Chang, J.K., Taur, J.I., Lo, Y.Y., Lee, W.L., Chang, C.S., Su, W.B., Wu, C.I.: A direct and polymer-free method for transferring graphene grown by chemical vapor deposition to any substrate. ACS Nano **8**(2), 1784–1791 (2014)
35. Liu, B., Feng, X., Zhang, S.M.: The effective Young's modulus of composites beyond the Voigt estimation due to the Poisson effect. Compos. Sci. Technol. **69**(13), 2198–2204 (2009)
36. Liu, G., Jin, W., Xu, N.: Graphene-based membranes. Chem. Soc. Rev. **44**(15), 5016–5030 (2015)
37. Lu, Q., Gao, W., Huang, R.: Atomistic simulation and continuum modeling of graphene nanoribbons under uniaxial tension. Model. Simul. Mater. Sci. Eng. **19**(5), 054006 (2011)
38. Lu, Q., Huang, R.: Nonlinear mechanics of single-atomic-layer graphene sheets. Int. J. Appl. Mech. **1**(03), 443–467 (2009)
39. Marianetti, C.A., Yevick, H.G.: Failure mechanisms of graphene under tension. Phys. Rev. Lett. **105**(24), 245502 (2010)
40. Mehralian, F., Firouzabadi, R.D.: A comprehensive continuum model for graphene in the framework of first strain gradient theory. Eur. Phys. J. Plus **136**(7), 1–15 (2021)
41. Miculescu, M., Thakur, V.K., Miculescu, F., Voicu, S.I.: Graphene-based polymer nanocomposite membranes: a review. Polym. Adv. Technol. **27**(7), 844–859 (2016)
42. Ni, Z., Bu, H., Zou, M., Yi, H., Bi, K., Chen, Y.: Anisotropic mechanical properties of graphene sheets from molecular dynamics. Physica B, Condens. Matter **405**(5), 1301–1306 (2010)
43. Papageorgiou, D.G., Kinloch, I.A., Young, R.J.: Mechanical properties of graphene and graphene-based nanocomposites. Prog. Mater. Sci. **90**, 75–127 (2017)

44. Patil, A., DasGupta, A.: Finite inflation of an initially stretched hyperelastic circular membrane. Eur. J. Mech. A, Solids **41**, 28–36 (2013)
45. Pelliciari, M., Pasca, D.P., Aloisio, A., Tarantino, A.M.: Size effect in single layer graphene sheets and transition from molecular mechanics to continuum theory. Int. J. Mech. Sci. **214**, 106895 (2022)
46. Pelliciari, M., Sirotti, S., Aloisio, A., Tarantino, A.M.: Analytical, numerical and experimental study of the finite inflation of circular membranes. Int. J. Mech. Sci. **226**, 107383 (2022)
47. Pelliciari, M., Tarantino, A.M.: Equilibrium paths for von Mises trusses in finite elasticity. J. Elast. **138**(2), 145–168 (2020)
48. Pelliciari, M., Tarantino, A.M.: Equilibrium paths of a three-bar truss in finite elasticity with an application to graphene. Math. Mech. Solids **25**(3), 705–726 (2020)
49. Pelliciari, M., Tarantino, A.M.: Equilibrium and stability of anisotropic hyperelastic graphene membranes. J. Elast. **144**(2), 169–195 (2021)
50. Pelliciari, M., Tarantino, A.M.: A nonlinear molecular mechanics model for graphene subjected to large in-plane deformations. Int. J. Eng. Sci. **167**, 103527 (2021)
51. Pumera, M.: Graphene-based nanomaterials for energy storage. Energy Environ. Sci. **4**(3), 668–674 (2011)
52. Qi, Z., Kitt, A.L., Park, H.S., Pereira, V.M., Campbell, D.K., Neto, A.C.: Pseudomagnetic fields in graphene nanobubbles of constrained geometry: A molecular dynamics study. Phys. Rev. B **90**(12), 125419 (2014)
53. Quanshui, Z., Boehler, J.P.: Tensor function representations as applied to formulating constitutive laws for clinotropic materials. Acta Mech. Sin. **10**(4), 336–348 (1994)
54. Raccichini, R., Varzi, A., Passerini, S., Scrosati, B.: The role of graphene for electrochemical energy storage. Nat. Mater. **14**(3), 271–279 (2015)
55. Rafiee, M.A., Rafiee, J., Wang, Z., Song, H., Yu, Z.Z., Koratkar, N.: Enhanced mechanical properties of nanocomposites at low graphene content. ACS Nano **3**(12), 3884–3890 (2009)
56. Saiz-Bretín, M., Domínguez-Adame, F., Malyshev, A.V.: Twisted graphene nanoribbons as nonlinear nanoelectronic devices. Carbon **149**, 587–593 (2019)
57. Shen, H., Zhang, L., Liu, M., Zhang, Z.: Biomedical applications of graphene. Theranostics **2**(3), 283 (2012)
58. Song, J., Kam, F.Y., Png, R.Q., Seah, W.L., Zhuo, J.M., Lim, G.K., Ho, P.K., Chua, L.L.: A general method for transferring graphene onto soft surfaces. Nat. Nanotechnol. **8**(5), 356–362 (2013)
59. Tao, L.Q., Zhang, K.N., Tian, H., Liu, Y., Wang, D.Y., Chen, Y.Q., Yang, Y., Ren, T.L.: Graphene-paper pressure sensor for detecting human motions. ACS Nano **11**(9), 8790–8795 (2017)
60. Wang, D., Fan, S., Jin, W.: Graphene diaphragm analysis for pressure or acoustic sensor applications. Microsyst. Technol. **21**(1), 117–122 (2015)
61. Wang, M.C., Yan, C., Ma, L., Hu, N., Chen, M.W.: Effect of defects on fracture strength of graphene sheets. Comput. Mater. Sci. **54**, 236–239 (2012)
62. Wang, P., Gao, W., Cao, Z., Liechti, K.M., Huang, R.: Numerical analysis of circular graphene bubbles. J. Appl. Mech. **80**(4), 040905 (2013)
63. Wang, Q., Hong, W., Dong, L.: Graphene "microdrums" on a freestanding perforated thin membrane for high sensitivity MEMS pressure sensors. Nanoscale **8**(14), 7663–7671 (2016)
64. Wei, X., Fragneaud, B., Marianetti, C.A., Kysar, J.W.: Nonlinear elastic behavior of graphene: Ab initio calculations to continuum description. Phys. Rev. B **80**(20), 205407 (2009)
65. Xu, M., Paci, J.T., Oswald, J., Belytschko, T.: A constitutive equation for graphene based on density functional theory. Int. J. Solids Struct. **49**(18), 2582–2589 (2012)
66. Yang, W.H., Feng, W.W.: On axisymmetrical deformations of nonlinear membranes. J. Appl. Mech. **37**(4), 1002–1011 (1970)
67. Yanovsky, Y.G., Nikitina, E.A., Karnet, Y.N., Nikitin, S.M.: Quantum mechanics study of the mechanism of deformation and fracture of graphene. Phys. Mesomech. **12**(5–6), 254–262 (2009)
68. Yazdani, H., Hatami, K.: Failure criterion for graphene in biaxial loading–a molecular dynamics study. Model. Simul. Mater. Sci. Eng. **23**(6), 065004 (2015)
69. Yuan, J., Liu, X., Xia, H., Huang, Y.: Analytical solutions for inflation of pre-stretched elastomeric circular membranes under uniform pressure. Theor. Appl. Mech. Lett. **11**, 100243 (2021)
70. Zang, X., Zhou, Q., Chang, J., Liu, Y., Lin, L.: Graphene and carbon nanotube (CNT) in MEMS/NEMS applications. Microelectron. Eng. **132**, 192–206 (2015)
71. Zhao, H., Min, K., Aluru, N.R.: Size and chirality dependent elastic properties of graphene nanoribbons under uniaxial tension. Nano Lett. **9**(8), 3012–3015 (2009)
72. Zhu, S.E., Krishna Ghatkesar, M., Zhang, C., Janssen, G.C.A.M.: Graphene based piezoresistive pressure sensor. Appl. Phys. Lett. **102**(16), 161904 (2013)